Inorganic Chemistry

pubs.acs.org/IC Article

H_2*CHX*hox: Rigid Cyclohexane-Reinforced Nonmacrocyclic Chelating Ligand for [$^{nat/67/68}$Ga]Ga^{3+}

Xiaozhu Wang,[†] María de Guadalupe Jaraquemada-Peláez,[†] Yang Cao, Aidan Ingham, Cristina Rodríguez-Rodríguez, Jinhe Pan, Yongliang Wang, Katayoun Saatchi, Urs O. Häfeli, Kuo-Shyan Lin, and Chris Orvig*

Cite This: *Inorg. Chem.* 2020, 59, 4895−4908 Read Online

ACCESS | Metrics & More | Article Recommendations | Supporting Information

ABSTRACT: A rigid chiral acyclic chelator H_2*CHX*hox was synthesized and evaluated for Ga^{3+}-based radiopharmaceutical applications; it was compared to the previously reported hexadentate H_2hox to determine the effect of a backbone reinforced from adding a chiral 1S,2S-trans-cyclohexane on metal complex stability, kinetic inertness, and *in vivo* pharmacokinetics. NMR spectroscopy and theoretical calculation revealed that [Ga(*CHX*hox)]$^+$ showed a very similar coordination geometry to that of [Ga(hox)]$^+$, and only one isomer in solution was observed by NMR spectroscopy. Solution studies showed that the modification results in a significant improvement in the exceptionally high thermodynamic stability of [Ga(hox)]$^+$ with a 1.56 log unit increase in stability constant (logK_{ML} = 35.91(1)). More importantly, H_2*CHX*hox showed very fast Ga^{3+} complexation at physiological pH 7.4, and acid-assisted Ga^{3+} complex dissociation kinetic studies (pH 1) in comparison with H_2hox revealed a 50-fold increase of the dissociation half-life time from 73 min to 58 h. Fluorescence microscopy imaging study confirmed its cellular uptake and accumulation in endoplasmic reticulum and mitochondria. MTT studies indicated a quite low cytotoxicity of [Ga(*CHX*hox)]$^+$ over a large concentration range. Dynamic PET imaging studies showed no accumulation in muscle, lungs, bone, and brain, suggesting no release of free Ga^{3+} ions. [^{68}Ga][Ga(*CHX*hox)]$^+$ is cleared from the mouse via hepatobiliary and renal pathways. Compared to [^{68}Ga][Ga(hox)]$^+$, the increased lipophilicity of [^{68}Ga][Ga(*CHX*hox)]$^+$ enhanced heart and liver uptake and decreased kidney clearance. [^{67}Ga][Ga(*CHX*hox)]$^+$ SPECT/CT imaging and biodistribution study revealed good clearance from liver to gallbladder after 90 min and finally into feces after 5 h. No decomposition or transchelation was observed over the 5 h study. These results confirmed H_2*CHX*hox to be an obvious improvement over H_2hox and an excellent candidate in this new "ox" family for the development of radiopharmaceutical compounds.

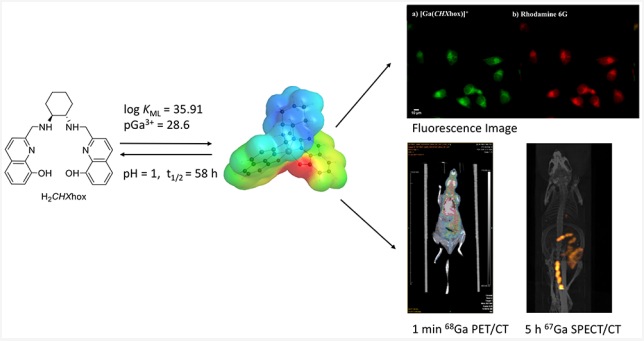

INTRODUCTION

^{68}Ga is a clinically important isotope with a short half-life time ($t_{1/2}$ = 68 min) and predominant β^+ decay yield (89%, 1.899 keV), suitable for imaging with small molecules and peptides.[1−4] ^{68}Ga based positron emission tomography (PET) imaging tracers have attracted increasing interest because of the commercially available ^{68}Ge/^{68}Ga generator system which can be used for more than 1 year due to the long half-life time of the parent ^{68}Ge ($t_{1/2}$ = 270 days) and allow cost-effective use of ^{68}Ga without the need for local cyclotron facilities.[5,6] The most successful samples currently are ^{68}Ga-labeled somatostatin analogues such as DOTATATE for neuroendocrine tumor (NET) imaging[7−14] and [^{68}Ga]Ga-PSMA (prostate specific membrane antigen) tracers including [^{68}Ga]Ga-HBED-CC-PSMA[15−21] and [^{68}Ga]Ga-PSMA I&T,[16,22−25] which have been studied widely and shown great potential in clinical imaging for prostate cancer diagnosis and staging.

Over the past decade, numerous Ga^{3+} chelators have been synthesized and tested for construction of ^{68}Ga-based tracers.[2,5,26−41] One major challenge is to maximize both rapid efficient radiolabeling under mild conditions (room temperature and near neutral pH) and high thermodynamic and kinetic stability, simultaneously.[42−45] Many fast-labeling acyclic chelators suffer from their poor kinetic inertness compared with macrocyclic chelators such as DOTA, whereas

Received: January 16, 2020
Published: March 16, 2020

https://dx.doi.org/10.1021/acs.inorgchem.0c00168
Inorg. Chem. 2020, 59, 4895−4908

Chart 1. Structures of DOTA, NOTA, DTPA, *CHX*-A″-DTPA, H_2dedpa, H_2*CHX*dedpa, [^{67}Ga(dedpa-D8)]$^+$, and [^{67}Ga(dedpa-D9)]$^+$ and Design Paradigm for H_2*CHX*hox

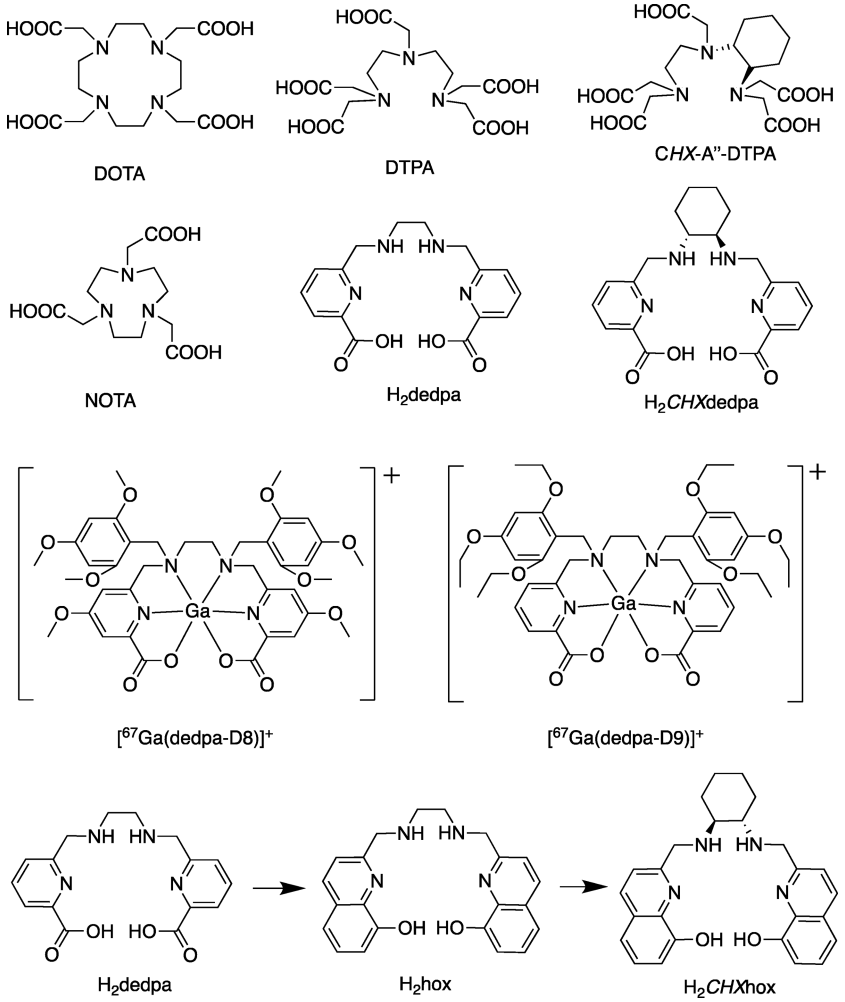

the latter are limited by slow coordination kinetics and therefore require extended labeling times and elevated temperatures, conditions incompatible with thermally sensitive biovectors.

In a recent report, an oxine (8-hydroxyquinoline)-based chelator, H_2hox, showed promise for kit-based pharmaceuticals.[41] H_2hox complexes Ga^{3+} over a broad pH range (1−11) with high log K_{ML} (34.4) and pM value (28.3), shows fast and quantitative ^{68}Ga labeling at mild conditions (5 min, RT), and yields high molar activity without purification. Even with the encouraging 73 min dissociation half-life time at pH 1, it cannot compare to the acidic kinetic inertness of macrocyclic chelators such as NOTA and DOTA that form intact complexes for days or weeks due to the reinforced fixed structure characteristic of macrocycles.[41] One important strategy to overcome this limitation of nonmacrocyclic chelators is to "preorganize" the flexible open chain structure by incorporating a rigid backbone group, decreasing the entropy penalty for wrapping it around the metal ion. A good example is *CHX*-A″-DTPA, which is derived from DTPA by adding a 1,2-trans-cyclohexanediamine backbone; this modification resulted in a markedly increased kinetic inertness while maintaining the acyclic character.[43,46−48] Therefore, in this work, an improvement in kinetic inertness and thermodynamic stability was attempted by incorporating a 1S,2S-transcyclohexanediamine backbone, following this strategy (Chart 1).

Moreover, adding a lipophilic cyclohexanediamine backbone may result in different pharmacokinetics and biodistribution of the tracers *in vivo*, thus a comprehensive evaluation including subcellular distribution, *in vitro* cytotoxicity, *in vivo* imaging, stability, and biodistribution was undertaken and the results compared with those of the previous generation. A few questions left unanswered in our previous study,[41] for example, the final clearance of the activity from the liver, are discussed here as well.

RESULTS AND DISCUSSION

H_2hox is the most successful acyclic chelator for gallium labeling from our past 10 years of study. In this work, H_2*CHX*hox, a more preorganized ligand, was designed by incorporating a 1S,2S-transcyclohexanediamine backbone to H_2hox as shown in Chart 1. H_2*CHX*hox is a preorganized structure, perhaps the most rigid nonmacrocyclic chelator ever reported, with only two carbons as flexible joints between the two rigid 8-hydroxyquinoline arms and the "fixed" backbone diamine. This structure is expected to mix the advantages of both acyclic and macrocyclic chelators, achieving fast labeling and excellent kinetic inertness simultaneously.

https://dx.doi.org/10.1021/acs.inorgchem.0c00168
Inorg. Chem. 2020, 59, 4895−4908

Synthesis and Characterization. The racemic mixture of H_2*CHX*hox has been tested as a chelator for the mobilization of iron from cells;[49] however, the single enantiomer has not been prepared and its chelation properties have not been investigated until this report. Herein, as in the modified synthetic route of H_2hox,[41,50] enantiomerically pure H_2*CHX*hox was prepared by reductive amination of 8-hydroxyquinoline-2-aldehyde and 1S,2S-transcyclohexanediamine in one step (Scheme 1). The crude product precipitated

Scheme 1. Synthesis of H_2*CHX*hox: (a) CH_3OH, 60°C, 4 h; (b) CH_3OH, $NaBH_4$ (5 equiv.), Overnight

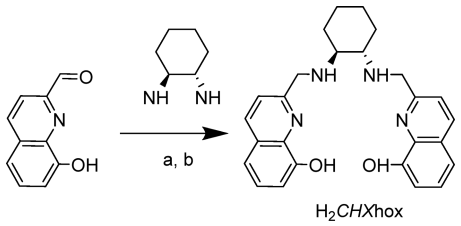

out of solution after the reaction was quenched with HCl (6 M) and neutralized with NaOH (2 M). After washing with H_2O and methanol, a pure product was obtained with a total yield of 83%. Both starting materials were cheaply purchased from a commercial supplier. Grams of ligand are prepared quickly and economically, which easily enables further investigation and future application of H_2*CHX*hox. As shown in Figure 1, the ^{1}H NMR spectrum of H_2*CHX*hox revealed the expected C2 symmetry with half-integrations of the resonances present, the incorporation of the chiral cyclohexane ring results in a typical diastereotopic splitting of protons (Figure 1, protons H and I) that observed α to the chiral center. This also agrees with the previously reported ^{1}H NMR spectrum of H_2*CHX*dedpa.[51]

Preparation and Characterization of Metal Complexes. H_2*CHX*hox and $Ga(ClO_4)_3$ were mixed in a 1:1 molar ratio in methanol and the pH was adjusted to around 6 using NaOH (0.1 M), the mixture was stirred for 1 h at 50 °C to ensure a thorough reaction. [Ga(*CHX*hox)][ClO_4] was then extracted by CH_2Cl_2 and dried in vacuo to obtain a yellow crystalline powder as the final product. The ^{1}H NMR spectrum confirmed the metal complex formation. As shown in Figures 1 and 2, before complexation, diastereotopic protons (F) on the free ligand (Figure 1) show small difference in chemical shift due to fast rotation. On binding to Ga^{3+} (Figure 2), they show a larger difference in chemical shift due to the formation of a relatively rigid 5-member chelate ring (N−C−C−N-Ga) and give a nice clean AB spin system (J = −17.3 Hz) that is consistent with that in [Ga*CHX*dedpa][ClO_4].[51] The aromatic protons are shifted downfield in the metal complex (Figure 2) due to the decreased electron density on the hydroxyquinoline ring, which also confirms the binding of the two arms to the Ga^{3+}. Meanwhile proton G on the chiral carbon is shifted upfield by about 0.3 ppm because of the increase in shielding from the coordination bond Ga−N(en). This suggests the two backbone nitrogen atoms are also binding to the central Ga^{3+}. Recrystallization of this powder from a CH_2Cl_2/Et_2O mixture yielded very thin needle-shaped crystals but, regrettably, no single crystal was good enough for X-ray crystallography.

DFT Calculations. The coordination geometry of the [Ga(*CHX*hox)]$^+$ cation in aqueous solution was simulated using density functional theory (DFT) as shown in Figure 3. The calculated bond parameters are summarized in Table 1 and compared with those in [Ga(hox)]$^+$. Similar geometries and bond lengths are observed in the simulated solution structures of both cations. The geometry of [Ga(hox)]$^+$ is symmetric as suggested by the equal bond lengths of the two set of coordination atoms, while the geometry of [Ga(*CHX*hox)]$^+$ is slightly asymmetric because of the rigid backbone.

Solution Studies. The protonation constants of H_2*CHX*hox were determined using UV-in-batch spectrophotometric titration as in the case of H_2hox.[41] The spectra collected during the titration (Figure S3) show the same spectral evolutions as H_2hox marked by the appearance of different isosbestic points. Analysis of the spectrophotometric data with the HypSpec2014 software[52] allowed the determination of the six protonation constants, the molar absorptivities of the different protonated species and the corresponding speciation plot (Table 2 and Figure S4). The largest variances in pK_a values of H_2*CHX*hox *vs.* H_2hox reside on the N_{ox} atoms of the

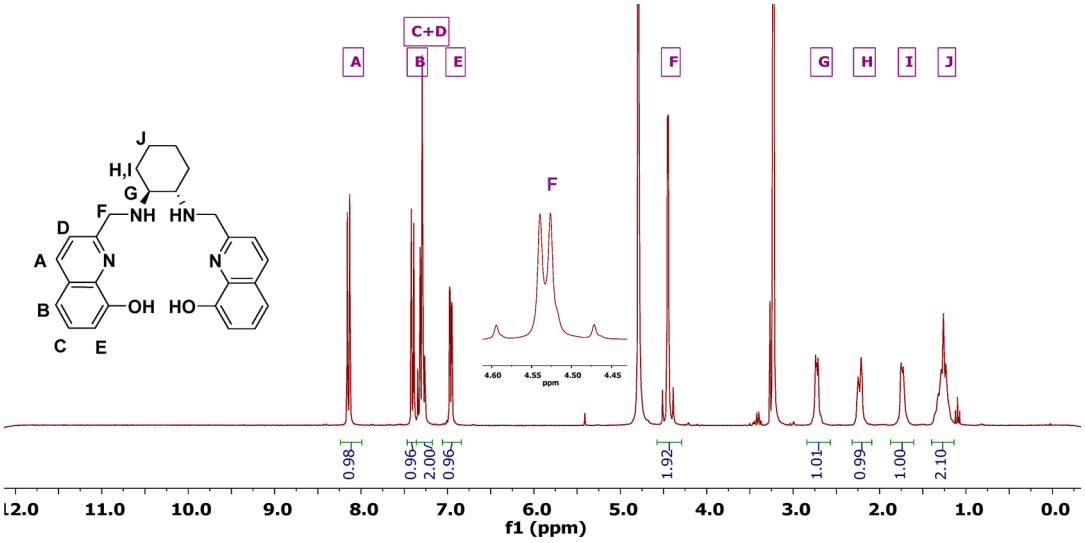

Figure 1. ^{1}H NMR spectrum of H_2*CHX*hox in MeOD (300 MHz, 25 °C).

https://dx.doi.org/10.1021/acs.inorgchem.0c00168
Inorg. Chem. 2020, 59, 4895−4908

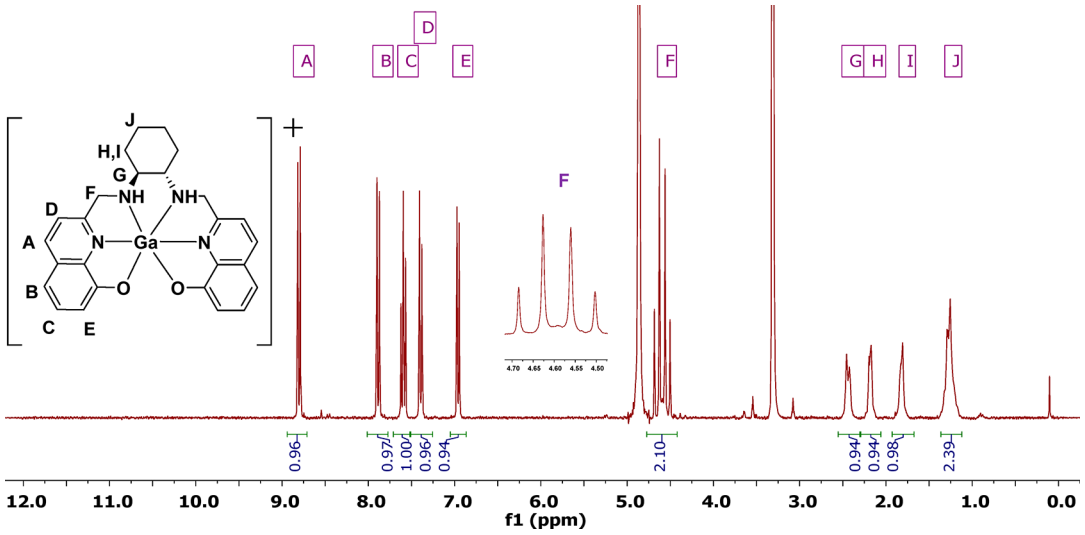

Figure 2. ^{1}H NMR spectrum of [Ga(*CHX*hox)][ClO_4] in MeOD (300 MHz, 25 °C).

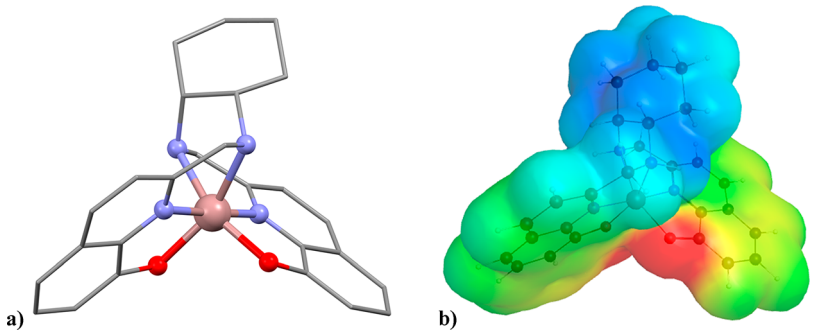

Figure 3. DFT calculated structure of (a) [Ga(*CHX*hox)]$^{+}$ with a hexacoordinated metal center (Ga^{3+}), and the electrostatic potentials of (b) [Ga(*CHX*hox)]$^{+}$ mapped onto electron density; the MEP represents a maximum potential of 0.02 au and a minimum of −0.25 au mapped onto electron density isosurface (0.002 e Å^{-3}, red to blue = negative to positive).

Table 1. Selected Calculated Bond Distances in the Cations [Ga(hox)]$^{+}$ and [Ga(*CHX*hox)]$^{+}$

[Ga(hox)]$^{+}$			[Ga(*CHX*hox)]$^{+}$		
atom	atom	length (Å)	atom	atom	length (Å)
Ga	O(ox)	1.943	Ga	O(ox)	1.969
Ga	O(ox)	1.943	Ga	O(ox)	1.965
Ga	N(ox)	1.990	Ga	N(ox)	1.992
Ga	N(ox)	1.990	Ga	N(ox)	1.989
Ga	N(en)	2.229	Ga	N(en)	2.169
Ga	N(en)	2.229	Ga	N(en)	2.181

Table 2. Protonation Constants of H_2*CHX*hox and H_2hox at 25°C

equilibrium reaction	H_2hox[a]	H_2*CHX*hox
$L + H^+ \leftrightarrows HL$	10.88(1)	10.87(1)
$HL + H^+ \leftrightarrows H_2L$	9.81(1)	9.84(1)
$H_2L + H^+ \leftrightarrows H_3L$	8.39(1)	8.75(1)
$H_3L + H^+ \leftrightarrows H_4L$	6.06(2)	5.95(1)
$H_4L + H^+ \leftrightarrows H_5L$	0.64(6)[b]	0.15(2)[b]
$H_5L + H^+ \leftrightarrows H_6L$	0.24(8)[b]	−0.36(3)[b]

[a]from ref.;[41] [b]in-batch-UV spectrophotometric titrations, not evaluated at constant I = 0.16 M NaCl. Charges are omitted for clarity.

quinoline units and a slight difference on the N_{en} atoms in the backbone. The increased rigidity in H_2*CHX*hox as well as the electrostatic repulsion between the protonated N atoms might favor the deprotonation of the N_{ox} atoms that could be stabilized by hydrogen bonding with the protonated N_{en} in the backbone. This may explain the lower pK_a values obtained for the H_6L^{4+} and H_5L^{3+} species: log K_6 = −0.36(3) and log K_5 = 0.15(2). The first deprotonation of the N_{en} atom, species H_4L^{2+} (log K_4 = 5.95(1)) in H_2*CHX*hox is fairly similar to that in H_2hox, whereas the second N_{en} deprotonation, species H_3L^{+} (log K_3 = 8.75(1)) is 0.36 units higher than the correspondent in H_2hox. The last deprotonation events are assigned to the phenol−OH groups, species H_2L and HL^{-} (log K_2 = 9.84(1) and log K_1 = 10.87(1)) are in good agreement with those of H_2hox.

H_2*CHX*hox complexation with Ga^{3+} metal ions was studied by following the spectral changes in the ligand absorption bands as the pH was raised from 0.19 to 11 by UV-in-batch spectrophotometry (Figure S5). The same studies were performed with H_2hox previously[41] and an equilibration time of 24 h was given to each sample before measurements were carried out. Except in the experiments with H_2*CHX*hox, the most acidic samples took 3 weeks to equilibrate until the spectra could be collected (Figure S5). The spectra of the Ga(III)-H_2*CHX*hox system collected from very acidic samples $H°$ −0.44 to pH 0.60 showed identical features to those of the

https://dx.doi.org/10.1021/acs.inorgchem.0c00168
Inorg. Chem. 2020, 59, 4895−4908

free ligand at the same pH values (Figures S3a, b and S5a, b). Complex formation starts from pH = 0.6, when a new band appears at λ = 368 nm as well as two isosbestic points at λ = 252 and 340 nm and the shift of the band of the free ligand at λ = 243 to 260 nm (Figure S5c, d). Any further transformation occurred as the pH was raised from 1.73 to 10.59. Analysis of the spectroscopic data, together with the molar absorption coefficients of the different absorbing species of the free ligand, allows the determination of the stability constant of the $[Ga(CHXhox)]^+$ complex via the use of the HypSpec program[52] (Figure S6 and Table 3). As shown in Table 3, the preorganized ligand $H_2CHXhox$ strongly complexes Ga^{3+} and an improved stability (δ log K_{ML} = 1.56) was obtained for the $[Ga(CHXhox)]^+$ complex compared with H_2hox. This is a significantly encouraging improvement considering that H_2hox is already one of the best Ga^{3+} chelators reported.

Table 3. Stability Constants (log *K*) of $H_2CHXhox$ and H_2hox Complexes with Ga^{3+}, and pM Values[a]

equilibrium reaction	$H_2CHXhox$	H_2hox
$M^{3+} + L \leftrightarrows ML$	35.91(1)[b]	34.35(1)[c]
pGa^{3+}	28.6	28.3

[a]pM is defined as $-\log [M]_{free}$ at [L] = 10 μM, [M] = 1 μM, pH 7.4. [b]In-batch acidic spectrophotometric competition at 25 °C and I = 0.16 M (NaCl). [c]From ref 41. Charges are omitted for clarity.

Acid-Assisted Dissociation and Formation Kinetics of Ga(III)-$H_2CHXhox$. Our previously reported chelating ligand H_2hox showed relatively poor acidic kinetic inertness compared with macrocyclic chelators such as DOTA, and one important goal in the design of $H_2CHXhox$ was to improve the kinetic inertness by introducing a reinforced backbone. Therefore, an acid-assisted dissociation kinetic study of the $[Ga(CHXhox)]^+$ complex was used to evaluate the improvement in the kinetic inertness. The study was performed by UV spectrophotometry at 25 °C and 0.1 M HCl. Standardized concentrated HCl was added to a Ga-*CHX*hox stock solution ($[Ga(CHXhox)][ClO_4]$ = 2.72 × 10^{-5} M) to achieve pH 1. The reaction was followed by monitoring the decrease of the complex absorption maxima band centered at 260 nm at 15 min intervals and 25 °C (Figure S7); only after 3 weeks was there no change on the absorption spectra and equilibrium completely achieved.

The UV spectra clearly show that there are no protonated complex species in the dissociation pathway by the presence of the well-defined isosbestic point at 252 nm previously depicted in the complex formation equilibria studies, and the complex dissociation leads to the ligand in its H_4L^{2+} species (Figures S3a and S7). A first-order rate constant was found as shown in Figure S7 and the half-life determined in those conditions was 57.8 h. This is around a 50-fold increase compared to the 73 min half-life of $[Ga(hox)]^+$ measured at the same conditions, confirming that the incorporation of a cyclohexane ring into the backbone not only increases the thermodynamic stability, but also greatly improves the kinetic inertness of the metal−ligand complex. Notwithstanding the high 57.8 h half-life (pH 1) found for the $[Ga(CHXhox)]^+$ complex with respect to 73 min for the $[Ga(hox)]^+$ analogue, it is still far from the half-lives for Ga(III) complexes formed with macrocyclic chelators such as DOTA (68 days, pH 1).[53] The most acidic *in vivo* environment is in the stomach with a pH around 1.5−3.5, whereas most of the other *in vivo* environments have a pH between 4.5 and 8.5. Therefore, the long half-life of $[Ga(CHXhox)]^+$ measured at pH 1 actually predicts an excellent *in vivo* kinetic inertness.

Gallium(III) complexes formed by macrocyclic chelators like DOTA, despite having high thermodynamic stability and kinetic inertness, suffer from slow complexation rates, which often limits their use with thermally sensitive biovectors. $H_2CHXhox$, an acyclic reinforced chelating ligand was expected to maintain the nature of acyclic chelators for fast metal complexation. In order to prove the fast Ga^{3+} complexation of $H_2CHXhox$, two formation kinetic experiments were performed. The first experiment was carried out at 1:1 metal to ligand molar ratio at pH 3.2 and 25 °C. From the spectra in Figure S8, it can be seen the free ligand with λ_{max} = 243 nm and the Ga−$H_2CHXhox$ solution at the same pH in which two new bands at λ_{max} = 260 and 370 nm appear as the

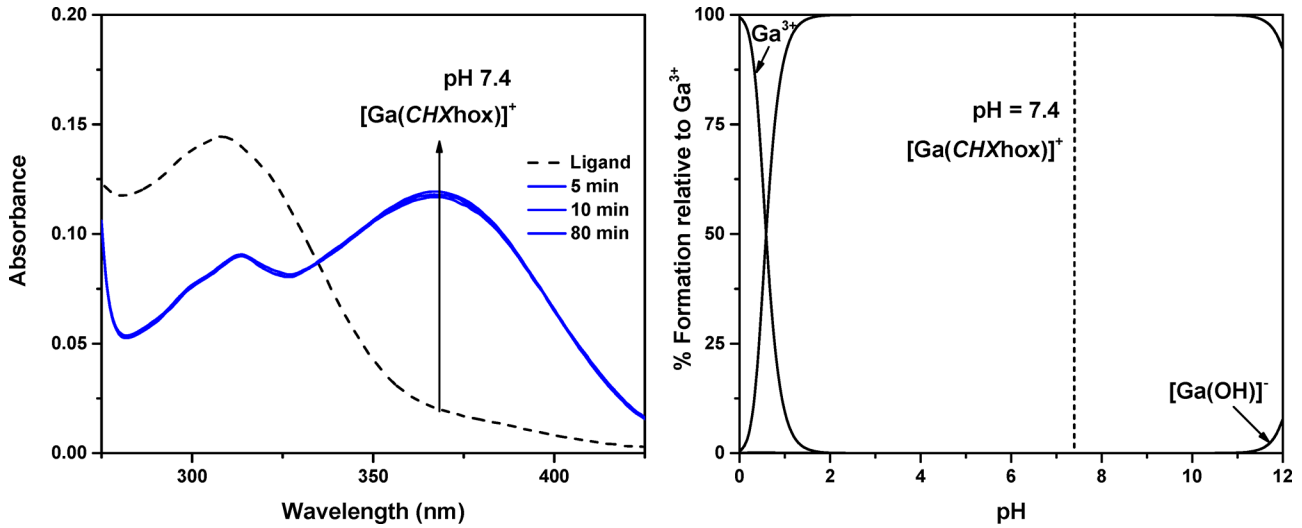

Figure 4. Formation kinetic experiment of $[Ga(CHXhox)]^+$. $[H_2CHXhox] = [Ga^{3+}]$ = 2.72 × 10^{-5} M, PBS × 1 buffer, pH 7.4, T = 25 °C (left). Speciation plot for Ga^{3+}-$H_2CHXhox$ under equilibrium conditions ($C_L = C_{Ga}$ = 0.001 M, UV in-batch titrations). The dashed line indicates pH 7.4 (right).

https://dx.doi.org/10.1021/acs.inorgchem.0c00168
Inorg. Chem. 2020, 59, 4895−4908

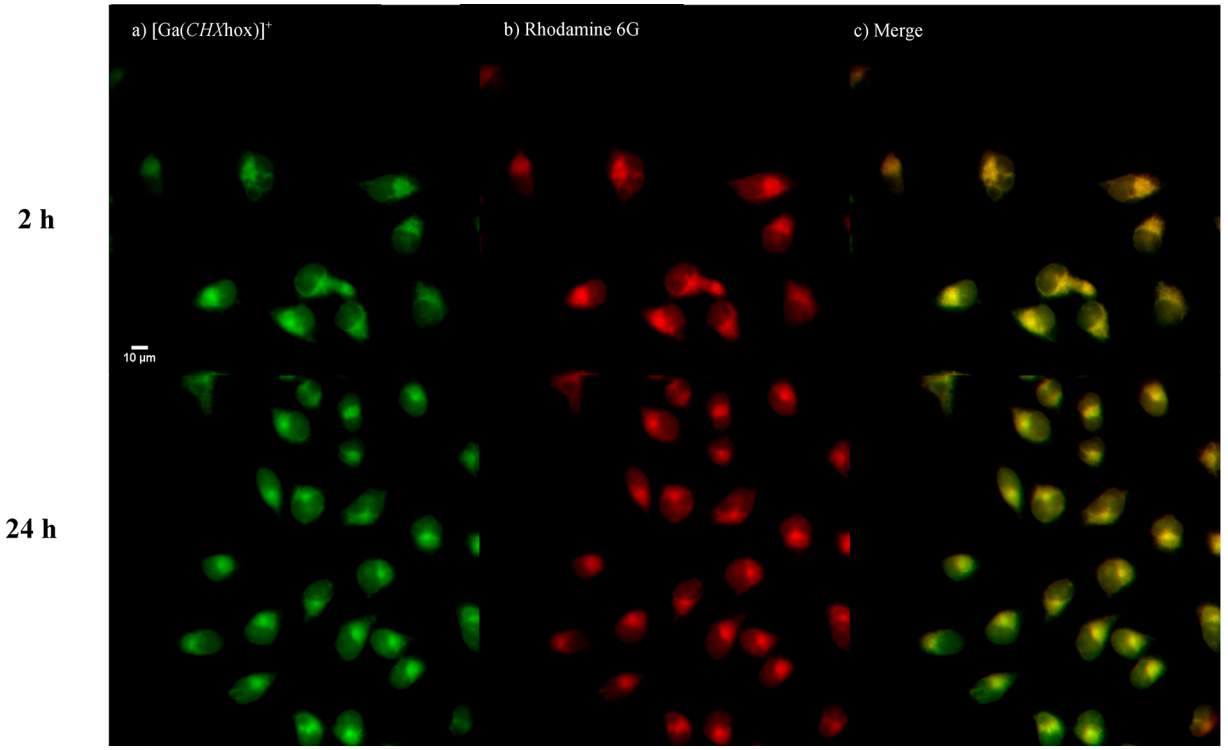

Figure 5. Fluorescence microscopy images from HeLa cells treated with(a) $[Ga(CHXhox)]ClO_4$ and (b) rhodamine 6G and (c) merged image. The scale is 10 μm.

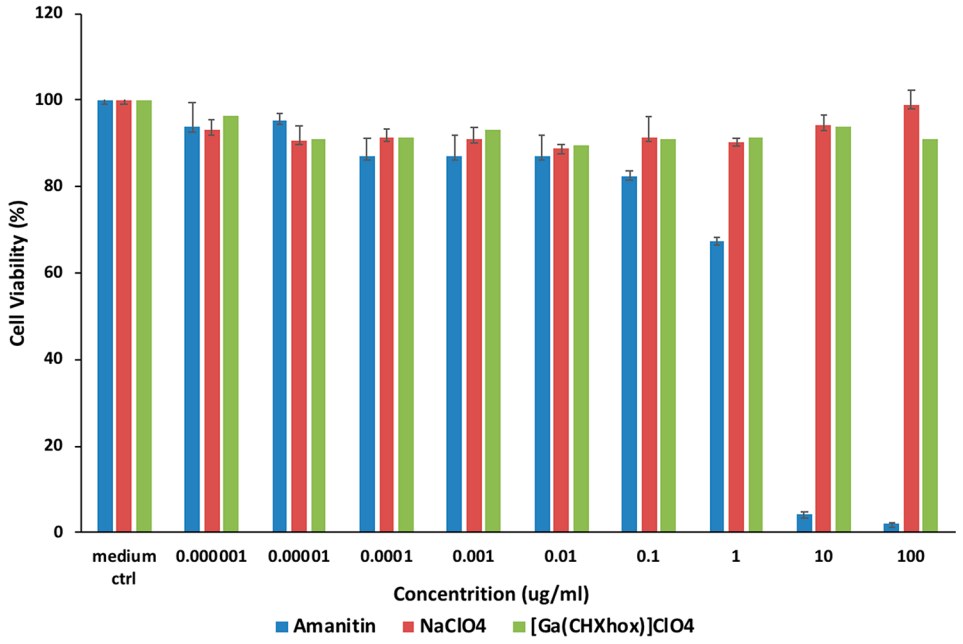

Figure 6. Dose dependent cytotoxicity of $[Ga(CHXhox)]ClO_4$ (green), Amanitin (blue, positive control) and $NaClO_4$ (red, negative control) on CHO cells.

metal complex forms. In this case, 70−80 min are required to fully form the complex.

The second experiment shows the spectra of the free ligand in PBS buffer (pH 7.4) and 25 °C and the Ga−H_2*CHX*hox solution in the same conditions (Figure 4 and Figure S9). It is clear from this experiment and in comparison with that at pH 3.2 that the metal complex formation is very fast and from $t = 0$ min the $[Ga(CHXhox)]^+$ complex is formed. As might have been expected for this reinforced chelator, the kinetics of complex formation is pH dependent.

In light of these experiments, the advantage on Ga^{3+} complexation at physiological pH 7.4 and 25 °C of this open chain chelating ligand H_2*CHX*hox is emphasized versus the macrocycle "gold standard" DOTA. Although the kinetic inertness of $[Ga(CHXhox)]^+$ at pH 1 is far from that of $[Ga(H_2DOTA)]^{2+}$, the superior formation kinetics at physiological pH, together with the existence of only one ML

https://dx.doi.org/10.1021/acs.inorgchem.0c00168
Inorg. Chem. 2020, 59, 4895−4908

complex species [Ga(*CHX*hox)]$^+$ in the pH range 1−11 (Figure 4), make the [Ga(*CHX*hox)]$^+$ complex worthy for further [$^{67/68}$Ga]Ga^{3+} *in vitro* and *in vivo* studies.

In Vitro Cellular Imaging. H_2*CHX*hox shows chelation-enhanced fluorescence properties (Figure S10) originating from the 8-hydroxyquinoline arm. In our previous paper, we carried out a proof of concept study showing that the intrinsic fluorescence enables direct imaging of the complex without an extraneous fluorescence and found that [Ga(hox)]$^+$ may accumulate in the cytoplasm of the cells. Herein, we further investigated the subcellular distribution of [Ga(*CHX*hox)]$^+$ in living HeLa cells by colocalization experiment with rhodamine 6G, a specific endoplasmic reticulum (ER) and mitochondria fluorescent dye. HeLa cells were incubated with 100 μM [Ga(*CHX*hox)][ClO_4]for 2 and 24 h, respectively, before fixing and staining with rhodamine 6G for 15 min. Bright field images of treated cells (Figure S11) taken prior to fluorescence imaging verified the cells as viable. The fluorescence imaging was taken with a 600 nm emission filter that allowed the detection of fluorescence at wavelengths >600 nm (Figure 5). No obvious decomposition of the [Ga(*CHX*hox)]ClO_4 complex was observed within the 24 h cellular environment, as the fluorescence intensity was constant and the free ligand would otherwise exhibit markedly lower fluorescence intensity at wavelengths above 600 nm (Figure 5 and Figure S10). The complex was found to colocalize with rhodamine 6G, suggesting that the complex was taken up by the cells and accumulates in ER and mitochondria which could be explained by the fact that both [Ga(*CHX*hox)] and rhodamine 6G are lipophilic monocations of small size. This preliminary investigation sets the basis for further detailed studies in the future because good cellular uptake and mitochondria accumulation could be an important characteristic for the design of a molecular imaging tracer.

In Vitro Cytotoxicity. In the fluorescence imaging study, the morphology of HeLa cells appeared normal and suggested low cellular toxicity. The cytotoxicity of [Ga(*CHX*hox)]ClO_4 was then further evaluated *in vitro* on CHO (Chinese hamster ovary) cells over a 72 h incubation using the MTT assay, with $NaClO_4$ as a negative control and amanitin toxin as positive control. As shown in Figure 6, [Ga(*CHX*hox)]ClO_4 did not show significant toxicity compared to the medium and the negative control $NaClO_4$ in a range of concentrations from 1×10^{-6} to 100 μg/mL. Even though higher concentrations cannot be tested due to the solubility limitation, this result already suggests a quite low cytotoxicity in the concentration range of *in vitro* fluorescence cellular studies and nuclear medicine applications.

Log $D_{7.4}$ Measurements and Mouse Plasma Competition Experiments. As previously reported, [^{68}Ga][Ga(hox)]$^+$, although more lipophilic than DOTA and H_2dedpa, was still a reasonably hydrophilic complex, with an average $logD_{7.4}$ of −0.47 ± 0.01 (n = 4).[41] To make a good comparison, the $LogD_{7.4}$ value of [^{68}Ga][Ga(*CHX*hox)]$^+$ was measured using the same conditions and showed that [^{68}Ga][Ga(*CHX*hox)]$^+$ is moderately lipophilic, with an average $LogD_{7.4}$ of 0.43 ± 0.03 (n = 4). This result confirmed that addition of a cyclohexane ring to the backbone converts the cation from slightly hydrophilic to moderately lipophilic, which can facilitate penetration through the cell membrane.[54] The *in vitro* stability of [^{68}Ga][Ga(*CHX*hox)]$^+$ was evaluated through a mouse plasma competition experiment as well. [^{68}Ga][Ga(*CHX*hox)]$^+$ was analyzed by radio-HPLC after incubation with mouse plasma for 5, 15, 30, and 60 min at 37 °C. As shown in Table 4 and Figure S10, the complex stayed completely intact (>99%) at all-time points, revealing its excellent *in vitro* stability of a whole half-life.

Table 4. Mouse Plasma Stability of [^{68}Ga][Ga(*CHX*hox)]$^+$

	5 min	15 min	30 min	1 h
[^{68}Ga][Ga(*CHX*hox)]$^+$	>99%	>99%	>99%	>99%

In Vivo Imaging. The high thermodynamic stability constant and kinetic inertness found for [Ga(*CHX*hox)]$^+$ in the solution studies, in combination with the excellent *in vitro* stability (in plasma competition experiments), suggest a high stability within an *in vivo* environment. Dynamic PET/CT imaging in mice was used to investigate the *in vivo* stability and biodistribution of the [^{68}Ga][Ga(*CHX*hox)]$^+$ cation. As shown in Figure 7a, b and Figure S13 (and similar to [^{68}Ga][Ga(hox)]$^+$), dynamic PET/CT imaging showed quick heart uptake in the first two minutes, and then clearance via both hepatobiliary (liver, then gastrointestinal tract) and renal (kidney, then bladder) pathways, which could be explained by the amphiphilic character of the cation. The clearance from the renal pathway is really fast; activity in the kidney showed up in just around 2.5 min postadministration. This is not surprising given the small size of the complex cation. The clearance from the hepatobiliary pathway is a little bit slower. The activity in the liver increased in the first 10 min and then started to excrete into the gastrointestinal tract after around 20 min. There is no leakage of free Ga^{3+}, which would otherwise combine with transferrin, resulting in relatively high vascular radioactivity, and mild bone marrow radioactivity.[55,56] Very low accumulation in muscle, lungs and brain was observed. These results suggest [^{68}Ga][Ga(*CHX*hox)]$^+$ has excellent *in vivo* stability and is worth further developing for use as a bifunctional tracer.

The activities found in different organs were then extracted from the PET/CT imaging data and were compared with the data from our previous [^{68}Ga][Ga(hox)]$^+$ PET/CT imaging study.[41] As shown in Figure 7b−e, the kidney uptake of [^{68}Ga][Ga(hox)]$^+$ is higher than the liver uptake, while in [^{68}Ga][Ga(*CHX*hox)]$^+$, the opposite trend was found with the activity in the liver being 1.5 times higher than that found in the kidneys. This could be explained by the increased lipophilicity from [^{68}Ga][Ga(hox)]$^+$ to [^{68}Ga][Ga(*CHX*hox)]$^+$ due to the cyclohexane ring addition. More importantly, the heart uptake and retention also showed an expected increase, agreeing with the previous finding that the lipophilic cations show better heart uptake and retention and may be useful for myocardial perfusion imaging.[57−60] Generally, high liver uptake is not a good characteristic for a myocardial perfusion tracer because the liver activity may disturb the interpretation of the heart activity in the inferior and left ventricular wall.[61] Therefore, to make a better comparison and evaluation, the heart/liver ratio was calculated and compared with H_2dedpa derivatives reported before.[58,62] As shown in Table 5, [^{68}Ga][Ga(*CHX*hox)]$^+$ showed a higher heart/liver ratio in the first 2 min than did [^{68}Ga][Ga(hox)]$^+$, whereas at 30 and 60 min time points, there are no obvious differences between them because the heart and liver uptake increments are almost equal. When compared with [^{67}Ga][Ga(dedpa-D8)]$^+$ (logP = 0.66) and [^{67}Ga][Ga(dedpa-D9)]$^+$ (log P = 1.10) (Chart 1 and Table 5),[58] the best twoH_2dedpa derivatives for

https://dx.doi.org/10.1021/acs.inorgchem.0c00168
Inorg. Chem. 2020, 59, 4895−4908

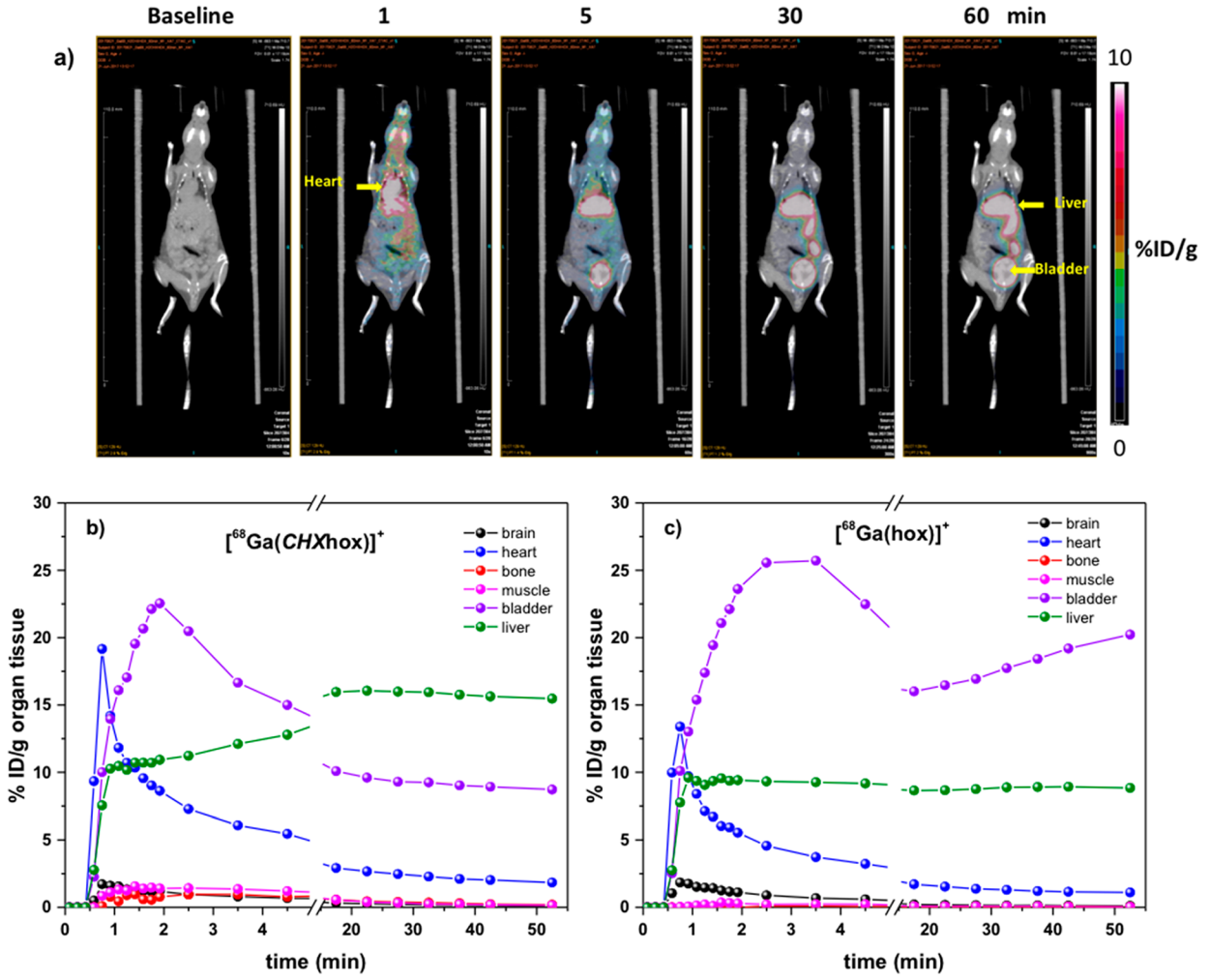

Figure 7. (a) PET/CT dynamic imaging of [^{68}Ga][Ga(*CHX*hox)]$^+$ and biodistribution of (b) [^{68}Ga][Ga(*CHX*hox)]$^+$ and (c) [^{68}Ga][Ga(hox)]$^+$ in male (NGR) mice.

Table 5. Heart/Liver Uptake Ratio of [^{68}Ga][Ga(hox)]$^+$, [^{68}Ga][Ga(*CHX*hox)]$^+$, [^{67}Ga][Ga(dedpa-D8)]$^+$ and [^{67}Ga][Ga(dedpa-D9)]$^+$.[58]

	heart/liver uptake ratio at different times (min)		
	2	30	60
[^{68}Ga][Ga(**hox**)]$^+$	0.588	0.146	0.124
[^{68}Ga][Ga(*CHX***hox**)]$^+$	0.790	0.143	0.119
[^{67}Ga][Ga(**dedpa-D8**)]$^+$	0.174	0.034	0.023
[^{67}Ga][Ga(**dedpa-D9**)]$^+$	0.16	0.11	0.07

myocardial imaging previously reported by us, [^{68}Ga][Ga(hox)]$^+$ and [^{68}Ga][Ga(*CHX*hox)]$^+$ showed a great improvement with a 4−6 fold increase in heart/liver ratio. This may be due to the smaller size of [^{68}Ga][Ga(hox)]$^+$ and [^{68}Ga][Ga(*CHX*hox)]$^+$ compared to [^{67}Ga][Ga(dedpa-D8)]$^+$ and [^{67}Ga][Ga(dedpa-D9)]$^+$, and therefore, it is easier for these smaller structures to undergo transmembrane diffusion into the heart muscle cells. The analysis from these data indicates that H_2hox and H_2*CHX*hox could be a good platform for the development of myocardial perfusion imaging tracers, even though it is really difficult to distinguish between myocardial activity and blood pool activity in the heart in the early time point.

Limited by the short half-life of [^{67}Ga]Ga^{3+}, the dynamic PET imaging was recorded for only 1 h, which is not long enough to assess the full hepatobiliary clearance profile. Therefore, [^{67}Ga][Ga(*CHX*hox)]$^+$ SPECT/CT imaging was also undertaken to monitor a longer time. As shown in the [^{67}Ga][Ga(*CHX*hox)]$^+$ SPECT/CT imaging (Figure 8), after 90 min, [^{67}Ga][Ga(*CHX*hox)]$^+$ showed good clearance from the liver while the gallbladder activity still remains high, indicating that [^{67}Ga][Ga(*CHX*hox)]$^+$ was secreted into the gastrointestinal tract via biliary excretion. This suggests that it can potentially be useful for gallbladder function imaging. For the renal clearance pathway, very weak signals were detected in kidney and most activity enters the bladder quickly. At 5 h, most of the activity entered into the gastrointestinal tract and feces and there is no obvious accumulation in both the liver and kidney, indicating that [^{67}Ga][Ga(*CHX*hox)]$^+$ has good metabolic and kinetic stability in the liver with no free metal ion released or transchelated.

Biodistribution of [^{67}Ga][Ga(*CHX*hox)]$^+$. The mice (n = 3) were then sacrificed for biodistribution study after 5 h imaging. As shown in Figure 9, consistent with imaging study results (Figures 7 and 8), negligible activity accumulated in blood, brain, bone, and muscle, further confirming excellent *in vivo* stability. Most of the activity was found in feces and urine

https://dx.doi.org/10.1021/acs.inorgchem.0c00168
Inorg. Chem. 2020, 59, 4895−4908

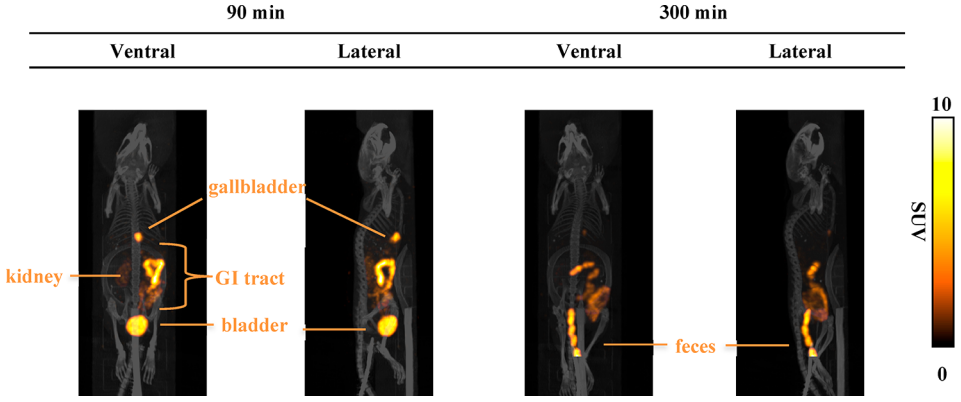

Figure 8. SPECT/CT imaging of $[^{67}Ga(CHXhox)]^+$.

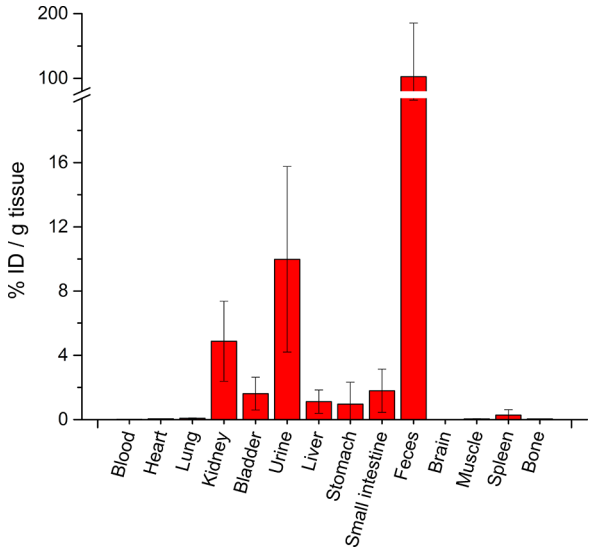

Figure 9. Biodistribution of $[^{67}Ga][Ga(CHXhox)]^+$ 5 h postinjection, $n = 3$. Percentage of injected dose per gram of organ weight.

suggesting a good clearance of this compound. The activity in feces is much higher than in urine.

Recent studies on $[^{68}Ga]$Ga-PSMA tracers revealed that using a more lipophilic chelator HBED-CC increased tumor uptake and *in vivo* imaging quality compared with the prominent DOTA conjugate.[39,63] Also in a recent study of $[^{68}Ga]$Ga-PSMA I&T tracer with hydrophilic chelator DOTA, a modification on the peptide structure using a naphthylalanine group to improve lipophilicity increased the PSMA affinity 3 times; however, further structural modifications using larger aromatic systems resulted in a 10-fold lower affinity because it impaired the interaction with the lipophilic binding pocket of PSMA.[64] This example indicates that using a lipophilic chelator may be an easy alternative compared with modification on the targeting molecules which may alter the binding affinity. Therefore, the lipophilic property of this new "oxine" based chelator system and its different pharmacokinetics and distribution compared with most previously reported chelators can provide a complementary choice in tracer design and modification and may have a positive impact on the pharmacokinetics of the final construct, especially for small molecules.

CONCLUSIONS

$H_2CHXhox$, a cyclohexane reinforced derivative of H_2hox, was designed, synthesized, and studied in solution showing that the thermodynamic stability of its Ga^{3+} complex was improved *vs.* the corresponding $[Ga(hox)]^+$ complex (log K_{ML} = 35.91(1) *vs.* 34.35(1)). More importantly, in acid-assisted Ga^{3+} complex dissociation kinetic studies, the dissociation half-life time was increased 50-fold from 73 min to 58 h, proving excellent kinetic inertness in acidic media. Complex formation kinetics experiments showed a pH-dependent behavior and at physiological pH 7.4 and 25 °C the complexation reaction is complete at t = 0 min, showing the great advantage for kit-based radiopharmaceuticals. Fluorescence microscopy imaging proved that the complex is taken up by cells and accumulates in ER and mitochondria. MTT studies indicate a low cytotoxicity over a large concentration range. Dynamic PET imaging studies showed very low accumulation in muscle, lungs and brain, suggesting high *in vivo* stability. $[^{68}Ga][Ga(CHXhox)]^+$ is quickly cleared from the mouse via hepatobiliary and renal pathways. Compared to $[^{68}Ga][Ga(hox)]^+$, $[^{68}Ga][Ga(CHXhox)]^+$ showed increased heart and liver uptake and decreased kidney clearance due to the increased lipophilicity. $[^{67}Ga][Ga(CHXhox)]^+$ SPECT/CT imaging and biodistribution study confirmed good clearance from liver to gallbladder after 90 min, and finally into feces after 5 h. No decomposition or transchelation was observed during the 5 h study. All these characteristics confirmed $H_2CHXhox$ to be an obvious improvement compared with H_2hox and could be an excellent alternative in this new "ox" family. Both $[^{68}Ga][Ga(hox)]^+$ and $[^{68}Ga][Ga(CHXhox)]^+$ exhibit a greatly improved heart/liver uptake ratio compared with $[^{67}Ga]$Ga(dedpa-D8) and $[^{67}Ga]$Ga(dedpa-D9), the previous reported H_2dedpa derivatives designed by our group for heart imaging, probably due to the increased lipophilicity and small size. The high activity of $[^{67}Ga][Ga(CHXhox)]^+$ in gallbladder at 90 min also suggests that it can be potentially useful in gallbladder and bile duct function imaging. Therefore, $H_2CHXhox$ is a very promising chelating ligand for the development of kit-based radiopharmaceuticals. Further modified derivatives are being prepared and undergoing investigation now.

EXPERIMENTAL SECTION

Materials and Methods. All solvents and reagents were purchased from commercial sources (TCI America, Sigma-Aldrich, Fisher Scientific) and were used as received unless otherwise indicated. The analytical thin-layer chromatography (TLC) plates

https://dx.doi.org/10.1021/acs.inorgchem.0c00168
Inorg. Chem. 2020, 59, 4895−4908

used were aluminum-backed ultrapure silica gel 60 Å, 250 μm thickness; ^{1}H and ^{13}C NMR spectra were recorded at ambient temperature on Bruker Avance 300 and Avance 400 spectrometers. The ^{1}H NMR spectra were calibrated against respective residual protio-solvent peaks, and the ^{13}C NMR spectra were referenced to the deuterated solvent. Low-resolution mass spectrometry was performed on a Waters ZG spectrometer with an ESCI (electrospray/chemical-ionization) source, and high-resolution electrospray ionization mass spectrometry (ESI-MS) was performed on a Micromass LCT time-of-flight (TOF) instrument. Microanalyses for C, H, and N were performed on a Carlo Erba Elemental Analyzer EA 1108. [^{68}Ga]Ga^{3+} was obtained from an Eckert & Ziegler (Berlin, Germany) IGG100 [^{68}Ga]Ga^{3+} generator and was purified according to the previously published procedures[65] using DGA resin column. Radioactivity of [^{68}Ga][Ga(*CHX*hox)]$^{+}$ was measured using a Capintec (Ramsey, NJ) CRC −25R/W dose calibrator. Purification and quality control of [^{68}Ga][Ga(*CHX*hox)]$^{+}$ were performed on an Agilent HPLC system equipped with a model 1200 quaternary pump, a model 1200 UV absorbance detector, and a Bioscan (Washington, DC) NaI scintillation detector. The radiodetector was connected to a Bioscan B-FC-1000 Flow-count system, and the output from the Bioscan Flow-count system was fed into an Agilent 35900E Interface which converted the analog signal to digital signal. The operation of the Agilent HPLC system was controlled using the Agilent ChemStation software. The HPLC columns were a semipreparative column (Phenomenex C18, 5 μ, 250 × 10 mm) and an analytical column (Phenomenex C18, 5 μ, 250 × 4.6 mm); the HPLC solvents were A: H_2O containing 0.1% TFA, and B: CH_3CN containing 0.1% TFA. PET imaging experiments were conducted using a Siemens (Erlangen, Germany) Inveon microPET/CT scanner.

Syntheses and Characterization. *H_2CHXhox (1).* 8-Hydroxyquinoline-2-carboxaldehyde (2.00 g, 11.6 mmol) was dissolved in 50 mL methanol and 1S,2S-transcyclohexanediamine (696 μL, 5.8 mmol) dissolved in 5 mL methanol was added dropwise; the reaction mixture was stirred at 60 °C for 4 h. A light-yellow precipitate formed, was collected and resuspended in 50 mL methanol. Eight equivalents of $NaBH_4$ (3.50 g, 92.8 mmol) were added in portions and the reaction mixture was stirred at room temperature overnight. HCl (20 mL, 6 M) was added and the reaction mixture stirred for 4 h. The pH of the reaction mixture was then readjusted to neutral using NaOH (2 M) and the off-white precipitate was collected by filtration and dried as crude product. The crude product was further washed with water and methanol to obtain the pure product (2.05 g, 4.8 mmol), yield = 83%. ^{1}H NMR (300 MHz, MeOD, 25 °C) δ; 8.15 (d, *J* = 8.5 Hz, 1H), 7.40 (d, *J* = 8.5 Hz, 1H), 7.36−7.21 (m, 2H), 6.96 (dd, *J* = 6.9, 2.0 Hz, 1H), 4.58−4.30 (dd, 2H, *J* = −17.3 Hz), 2.81−2.60 (m, 1H), 2.23 (d, *J* = 10.7 Hz, 1H), 1.74 (d, *J* = 6.8 Hz, 0H), 1.28 (q, *J* = 9.3, 7.8 Hz, 2H). ^{13}C NMR (75 MHz, MeOD, 25 °C) δ; 157.1, 153.0, 137.9, 136.8, 128.3, 127.0, 120.9, 117.6, 111.0, 60.6, 50.4, 30.6, 24.7. HR-ESI-MS: calcd. for $[C_{26}H_{28}N_4O_2 + H]^{+}$, 429.2291; found, 429.2290.

[Ga(CHXhox)][ClO$_4$](2). H_2*CHX*hox (40 mg, 0.11 mmol) was dispersed in 5 mL methanol. $Ga(ClO_4)_3{\cdot}6H_2O$ (55 mg, 0.11 mmol) was added as a solid, and the pH was adjusted to ∼6 using 0.1 M NaOH. The reaction mixture was stirred for 1 h at 50 °C and 5 mL of H_2O was added after the solution had cooled to room temperature. CH_2Cl_2 (3 × 5 mL) was then added to extract the product and the organic phase was dried in vacuo to obtain a yellow crystalline powder as the final product. ^{1}H NMR (300 MHz, MeOD, 25 °C) δ; 8.80 (d, *J* = 8.5 Hz, 1H), 7.89 (d, *J* = 8.5 Hz, 1H), 7.59 (t, *J* = 8.1 Hz, 1H), 7.44−7.31 (dd, *J* = 7.8, 0.8 Hz, 1H), 6.96 (dd, *J* = 7.8, 0.8 Hz, 1H), 4.73−4.46 (dd, 2H), 2.44 (d, *J* = 10.4 Hz, 1H), 2.18 (d, *J* = 7.7 Hz, 1H), 1.81 (s, 1H), 1.27 (m, *J* = 12.1 Hz, 2H). HR-ESI-MS calcd. for $[C_{26}H_{26}{}^{69}GaN_4O_2]^{+}$, 495.1312; found, 495.1314.

DFT Calculations. All calculations were performed using the Gaussian 09 package (Revision D.01). Full geometry optimizations of [Ga(hox)]$^{+}$ were performed with the CAM-B3LYP hybrid exchange−correlation functional[66] in aqueous solution using the polarizable continuum model (PCE).[67] Geometry optimizations were carried out using the 6-31G(d,p) basis set on first and second row elements, and the Los Alamos effect core potential (ECP) and valence basis set of double-ζ quality (LANL2DZ) on the Ga atom.[68] The input coordinates of atoms were adapted from the MM refined structure of the [Ga(*CHX*hox)][ClO_4] complex from Avogadro and no constraints on symmetry were imposed during the geometry optimization. The resulting geometries showed no imaginary frequencies thus were confirmed to be minima on the potential energy surfaces.

Solution Thermodynamics. Protonation equilibria of the ligand and complex formation equilibria with Ga^{3+} ions were studied by UV spectrophotometric batch experiments as described before[41] using a Cary 60 UV−vis spectrophotometer in the spectral range 200−450 nm, at 25 °C and 1 cm path length (*l*). A set of 49 solutions containing the ligand (H_2*CHX*hox, 2.75 × 10^{-5} M) in water were prepared and different amounts of standardized HCl or NaOH were added to cover a range from H^0 −0.52 to pH 11.51. The ionic strength of each sample was adjusted (when possible) to 0.16 M by addition of different amounts of NaCl. In the most acidic samples (below pH 0.6), it was not possible to maintain constant ionic strength because that depends on the HCl content, and for those solution,s the correct acidity scale H^0 was used.[69] In the samples at pH <2, the equilibrium H^+ concentration was calculated from solution stoichiometry, and for the rest of the samples, pH was measured with a Ross combination glass electrode that was calibrated daily for hydrogen ion concentration using HCl as described before[70] and the results were analyzed by the Gran[71] procedure.

For the complex formation equilibria, the set of solutions was prepared in the same way as described above. For the Ga(III)-H_2*CHX*hox system, the set of samples was prepared by solving the corresponding yellow crystalline powder [Ga(*CHX*hox)][ClO_4]] (**2**). Equilibration time of 2 min for the ligand protonation equilibria study was allowed before measuring the pH and the UV absorption spectra. For the samples containing the Ga(III) complex, the measurements were performed only after 3 weeks because of the longer time to equilibrate for the most acidic samples. The spectral data were analyzed using the HypSpec2014 program.[52] Proton dissociation constants corresponding to hydrolysis of Ga(III) aqueous ions included in the calculations were taken from Baes and Mesmer.[72] The species formed in the studied systems are characterized by the general equilibrium: $pM + qH + rL = M_pH_qL_r$ (charges omitted). For convention, a complex containing a metal ion M, proton H, and ligand L has the general formula $M_pH_qL_r$. The stoichiometric indices *p* might also be 0 in the case of protonation equilibria, and negative values of *q* refers to proton removal or hydroxide ion addition during formation of the aqua complex. The overall equilibrium constant for the formation of the complexes $M_pH_qL_r$ from its components is designated as log *β*. Stepwise equilibrium constants log *K* correspond to the difference in log units between the overall constants of sequentially protonated (or hydroxide) species. A more straightforward comparison of the ability of different ligands to coordinate a specific metal ion than the thermodynamic stability constants alone, is the pM value, defined as $(-\log[M^{n+}]_{free})$ and is calculated at specific conditions ($[M^{n+}]$ = 1 μM, $[L^{x-}]$ = 10 μM, pH 7.4, and 25 °C), taking into consideration metal−ligand association and ligand basicity.[73]

For the complex formation kinetics experiments, samples of the free ligand and the metal complex were prepared at pH 3.2 by addition of standardized NaOH (0.15 M) and in PBS × 1 buffer (pH 7.4), $[Ga^{3+}]$ = [H_2*CHX*hox] = 2.72 × 10^{-5} M and the UV spectra were collected every 5 min, *l* = 1 cm, *T* = 25 °C.

Fluorescence Imaging. Hela cells were purchased from the American Type Culture Collection (ATCC). Cells were grown in Eagle's minimal essential medium (MEM) supplemented with heat-inactivated 10% fetal bovine serum, 1 mM sodium pyruvate, 4 mM L-glutamine, and 1% nonessential amino acids in a humidified incubator at 37 °C and 5% CO_2. Cells were seeded 8-well culture slips 24 h prior to treatment. The [Ga(*CHX*hox)][ClO_4]working solution for fluorescence microscopy was prepared from a PBS stock solution. No precipitation of the compound was observed in the working solution under this condition. Cells were exposed to 100 uM [Ga(*CHX*hox)]-

https://dx.doi.org/10.1021/acs.inorgchem.0c00168
Inorg. Chem. 2020, 59, 4895−4908

[ClO_4] for 2 and 24 h, washed with phosphate buffered saline (PBS) 3 times before fixed and stain with rhodamine 6G for 15 min. Bright-field images of treated cells (Figure S11) taken prior to fluorescence imaging verified the cells as viable and imaging was done using Olympus IX83 Inverted fluorescence microscope (with DIC optics, metal-halide lamp, fast filter wheels and dichoric turret, and sCMOS camera) and Cell-F fluorescence imaging software (Olympus).

In Vitro Cytotoxicity (MTT). Cell viability was assessed using a modified MTT assay.[74,75] [Ga(*CHX*hox)]ClO_4,$NaClO_4$ and amanitin toxin dissolved in MEM medium were added at various concentrations (1.0×10^{-6} μg/mL to 100 μg/mL) to CHO cells (1×10^4) in a 96-well culture plate. After 72 h of incubation at 37 °C in air with 5% CO_2, 50 μL of thiazolyl blue tetrazolium bromide (MTT, Sigma-Aldrich) solution (2.5 mg/mL) was added to the experimental wells, including control and the plates were incubated for 3 h at 37 °C. The wells were then aspirated and 150 μL of DMSO was added. The plate covers were removed and absorbance of the solution in each well, including the blank was read at a test wavelength of 570 nm. The average values were determined from triplicate readings subtracting the average value for blank.

[^{68}Ga][Ga(*CHX*hox)]$^+$ Labeling. The ^{68}Ga generator was eluted with a total of 4 mL of 0.1 mol/L HCl. The eluate that contained the radioactivity was mixed with 2 mL concentrated HCl. The mixture was passed through a DGA resin column and the column was washed with 3 mL of 5 M HCl. After the column was dried by the passage of air, the trapped [^{68}Ga]Ga^{3+} was eluted off with 0.5 mL water. Purified [^{68}Ga]Ga^{3+} in 0.5 mL water was added into a 4 mL glass vial preloaded with 0.7 mL of HEPES buffer (2 M, pH 5.0) and 25 nmol H_2*CHX*hox. The radiolabeling reaction was carried out under microwave heating for 1 min. The reaction mixture was purified by HPLC using the semipreparative column eluted with 79/21 A/B at a flow rate of 4.5 mL/min. The retention time of [^{68}Ga][Ga(*CHX*hox)]$^+$ was 20.2 min. The eluate fraction containing the radiolabeled product was collected, diluted with water (50 mL), and passed through a C18 Sep-Pak cartridge that was prewashed with ethanol (10 mL) and water (10 mL). After washing the C18 Sep-Pak cartridge with water (10 mL) the [^{68}Ga]Ga^{3+}-labeled product was eluted off the cartridge with ethanol (0.4 mL), dried by helium, and redissolved with saline (0.5 mL) for plasma stability and imaging studies. Quality control was performed using the analytical column eluted with 79/21 A/B at a flow rate of 2 mL/min. The retention time of [^{68}Ga][Ga(*CHX*hox)]$^+$ was 10.4 min (Figure S12). The decay-corrected isolated radiochemical yield was 68 ± 2% (n = 2) with a greater than 99% radiochemical purity. The average specific activity was 7.14 ± 0.77 GBq/nmol (n = 2).

log $D_{7.4}$ Measurements. Aliquots (2 μL) of the [^{68}Ga][Ga(*CHX*hox)]$^+$ were added to a vial containing 3 mL octanol and 3 mL 0.1 M phosphate buffer (pH 7.4). The mixture was vortexed for 1 min and then centrifuged for 10 min. Samples of the octanol (1 mL) and buffer (1 mL) layers were taken and counted. log $D_{7.4}$ was calculated using eq 1.

$$\log D_{7.4} = \log_{10}[(\text{counts in octanol phase})/(\text{counts in buffer phase})] \quad (1)$$

Stability in Mouse Plasma. Aliquots (20 μL) of [^{68}Ga][Ga(*CHX*hox)]$^+$ were incubated with 80 μL of mouse plasma for 5, 15, 30, and 60 min at 37 °C. At the end of each incubation period, samples were quenched with 100 μL 70% CH_3CN and centrifuged for 20 min. The metabolites were measured using a semipreparative HPLC system with the same HPLC conditions as described for the purification of [^{68}Ga][Ga(*CHX*hox)]$^+$.

PET/CT Imaging Studies. PET/CT imaging studies were conducted at BC Cancer in accordance with the guidelines established by the Canadian Council on Animal Care and approved by the Animal Ethics Committee of the University of British Columbia. Male NOD.Cg-Rag1^{tm1Mom}Il2rg^{tm1Wjl}/SzJ (NRG) mice were purchased from in-house colonies at the Animal Research Centre, BC Cancer Research Centre, Vancouver, Canada. PET/CT imaging experiments were conducted using a Siemens (Knoxville, TN, USA) Inveon microPET/CT scanner. Mice were sedated with 2% isoflurane in oxygen inhalation and positioned in the scanner. A baseline CT scan was obtained for localization and attenuation correction before radiotracer injection, using 80 kV X-rays at 500 mA, three sequential bed positions with 34% overlap, and 180-degree continuous rotation. The mice were kept warm by a heating pad during acquisition. The dynamic acquisition of 60 min was started at the time of intravenous injection with ∼3.4−4.0 MBq of [^{68}Ga*CHX*hox]$^+$. The list mode data were rebinned into time intervals (12 × 10 s, 8 × 60 s, 7 × 300 s, 1 × 900 s) to obtain tissue time-activity curves. Images were reconstructed using iterative three-dimensional ordered subset expectation maximization (OSEM3D, 2 iterations) using maximum a priori with shifted poisson distribution (SP-MAP, 18 iterations).

SPECT/CT Imaging Studies. These studies were performed at the Center for Comparative Medicine, UBC, in accordance with the Canadian Council on Animal Care (CCAC) and protocol approved by the Animal Care Committee (ACC) of the University of British Columbia (A16−0150). A solution of H_2*CHX*hox (2.34×10^{-5} M, 100 μL) was added to [^{67}Ga]$GaCl_3$ (44 MBq, 10 μL 0.1 M HCl). The solution was diluted by adding water (250 μL) and PBS (×10; 40 μL) to 400 μL total volume of PBS × 1 (pH 7.4). The mixture was then shaken in an Eppendorf shaker for 15 min at RT at 750 rpm. Radiochemical yield was over 97.1% by iTLC. The radiochemical purity was greater than 95%, and hence the radiotracer was not purified further. The molar activity without purification was 18.5 MBq/nmol. Three healthy C57Bl/6 female mice (∼16 g) were anaesthetized using isoflurane on a precision vaporizer (5% in oxygen for induction, between 1.5 and 2.5% in oxygen for maintenance) and received a subcutaneous injection of lactated Ringer's solution (0.5 mL) for hydration prior to each imaging scan. Dynamic whole-body images were acquired during 60 min using a multimodal SPECT/CT scanner (VECTor/CT, MILabs, The Netherlands) equipped with a XUHS-2 mm mouse pinhole collimator. Six frames of 10 min were acquired for the first hour scan. Following each SPECT acquisition, a whole-body CT scan was acquired to obtain anatomical information and both images were registered. For the SPECT images, 16 subsets, 10 iterations, and an isotropic 0.4 mm voxel grid were used. The images were decay-corrected and attenuation correction was applied after CT registration. For visual representation, the reconstructed volumes of SPECT scans were postfiltered with a 3D Gaussian filter. CT scans were acquired with a tube setting of 55 kV and 615 μA.

■ ASSOCIATED CONTENT

Supporting Information

NMR spectra (^{13}C); representative spectra of the in-batch UV-titration of H_2*CHX*hox and Ga^{3+}-*CHX*hox; speciation plots of H_2*CHX*hox and H_2hox; fit for the ligand titration UV-batch; fit for the batch titration of the Ga(III)-H_2*CHX*hox; dissociation kinetics of [Ga(*CHX*hox)]$^+$ complex; formation kinetic experiment of [Ga(*CHX*hox)]$^+$; fluorescence spectra of H_2*CHX*hox and its Ga^{3+} complex in PBS; bright field images of treated cells; radio-HPLC spectra of [^{68}Ga][Ga(*CHX*hox)]$^+$; PET/CT dynamic imaging of [^{68}Ga][Ga(*CHX*hox)]$^+$ The Supporting Information is available free of charge at https://pubs.acs.org/doi/10.1021/acs.inorgchem.0c00168.

(PDF)

■ AUTHOR INFORMATION

Corresponding Author

Chris Orvig − *Medicinal Inorganic Chemistry Group, Department of Chemistry, University of British Columbia, Vancouver, BC V6T 1Z1, Canada;* orcid.org/0000-0002-2830-5493; Email: orvig@chem.ubc.ca

https://dx.doi.org/10.1021/acs.inorgchem.0c00168
Inorg. Chem. 2020, 59, 4895−4908

Authors

Xiaozhu Wang − *Medicinal Inorganic Chemistry Group, Department of Chemistry, University of British Columbia, Vancouver, BC V6T 1Z1, Canada;* orcid.org/0000-0002-5882-0066

María de Guadalupe Jaraquemada-Peláez − *Medicinal Inorganic Chemistry Group, Department of Chemistry, University of British Columbia, Vancouver, BC V6T 1Z1, Canada;* orcid.org/0000-0002-6204-707X

Yang Cao − *Medicinal Inorganic Chemistry Group, Department of Chemistry, University of British Columbia, Vancouver, BC V6T 1Z1, Canada;* orcid.org/0000-0001-8636-7919

Aidan Ingham − *Medicinal Inorganic Chemistry Group, Department of Chemistry, University of British Columbia, Vancouver, BC V6T 1Z1, Canada; Life Sciences Division, TRIUMF, Vancouver, British Columbia V6T 2A3, Canada*

Cristina Rodríguez-Rodríguez − *Center for Comparative Medicine, Vancouver, British Columbia V6T 1W5, Canada; Department of Physics and Astronomy, University of British Columbia, Vancouver, British Columbia V6T 1Z1, Canada;* orcid.org/0000-0002-3313-4422

Jinhe Pan − *Department of Molecular Oncology, BC Cancer Research Centre, Vancouver, BC V5Z 1L3, Canada*

Yongliang Wang − *Department of Molecular Oncology, BC Cancer Research Centre, Vancouver, BC V5Z 1L3, Canada*

Katayoun Saatchi − *Faculty of Pharmaceutical Sciences, University of British Columbia, Vancouver, British Columbia V6T 1Z3, Canada;* orcid.org/0000-0002-5372-6791

Urs O. Häfeli − *Faculty of Pharmaceutical Sciences, University of British Columbia, Vancouver, British Columbia V6T 1Z3, Canada;* orcid.org/0000-0003-0671-4509

Kuo-Shyan Lin − *Department of Molecular Oncology, BC Cancer Research Centre, Vancouver, BC V5Z 1L3, Canada;* orcid.org/0000-0002-0739-0780

Complete contact information is available at: https://pubs.acs.org/10.1021/acs.inorgchem.0c00168

Author Contributions

†X.W. and M.d.G.J.-P. contributed equally to this work.

Funding

We gratefully acknowledge funding from NSERC CREATE IsoSiM at TRIUMF for a PhD research stipend (AI) and NSERC Discovery Grant (RGPIN-42394-13) as well as NSERC (CHRP 493725-16) and the Canadian Institutes of Health Research (CIHR, CPG-146482) as a Collaborative Health Research Project.

Notes

The authors declare no competing financial interest.

■ ACKNOWLEDGMENTS

M. V. Tran, Dr. Y. Wang, J. Chen, Dr. E. Polishchuk are thanked for their important assistance.

■ REFERENCES

(1) Clarke, E. T.; Martell, A. E. Stabilities of Trivalent Metal-Ion Complexes of the Tetraacetate Derivatives of 12-Membered, 13-Membered and 14-Membered Tetraazamacrocycles. *Inorg. Chim. Acta* **1991**, *190*, 37−46.

(2) Prata, M. I.; Santos, A. C.; Geraldes, C. F.; de Lima, J. J. Structural and in vivo studies of metal chelates of Ga(III) relevant to biomedical imaging. *J. Inorg. Biochem.* **2000**, *79*, 359−63.

(3) Tsionou, M. I.; Knapp, C. E.; Foley, C. A.; Munteanu, C. R.; Cakebread, A.; Imberti, C.; Eykyn, T. R.; Young, J. D.; Paterson, B. M.; Blower, P. J.; Ma, M. T. Comparison of macrocyclic and acyclic chelators for gallium-68 radiolabelling. *RSC Adv.* **2017**, *7*, 49586−49599.

(4) Uppal, R.; Ciesienski, K. L.; Chonde, D. B.; Loving, G. S.; Caravan, P. Discrete bimodal probes for thrombus imaging. *J. Am. Chem. Soc.* **2012**, *134*, 10799−802.

(5) Maecke, H. R.; Hofmann, M.; Haberkorn, U. (68)Ga-labeled peptides in tumor imaging. *J. Nucl. Med.* **2005**, *46* (Suppl 1), 172S−8S.

(6) Shetty, D.; Lee, Y. S.; Jeong, J. M. (68)Ga-labeled radiopharmaceuticals for positron emission tomography. *Nucl. Med. Mol. Imaging* **2010**, *44*, 233−40.

(7) Kunz, W. G.; Eschbach, R. S.; Stahl, R.; Kazmierczak, P. M.; Bartenstein, P.; Rominger, A.; Auernhammer, C. J.; Spitzweg, C.; Ricke, J.; Cyran, C. C. Identification and characterization of myocardial metastases in neuroendocrine tumor patients using 68Ga-DOTATATE PET-CT. *Cancer Imaging* **2018**, *18*, 34.

(8) Hoberuck, S.; Michler, E.; Zophel, K.; Platzek, I.; Kotzerke, J.; Brogsitter, C. Brain Metastases of a Neuroendocrine Tumor Visualized by 68Ga-DOTATATE PET/CT. *Clin. Nucl. Med.* **2019**, *44*, 50−52.

(9) Zhang, P.; Yu, J.; Li, J.; Shen, L.; Li, N.; Zhu, H.; Zhai, S.; Zhang, Y.; Yang, Z.; Lu, M. Clinical and Prognostic Value of PET/CT Imaging with Combination of (68)Ga-DOTATATE and (18)F-FDG in Gastroenteropancreatic Neuroendocrine Neoplasms. *Contrast Media Mol. Imaging* **2018**, *2018*, 2340389.

(10) Calais, J.; Czernin, J.; Eiber, M.; Fendler, W. P.; Gartmann, J.; Heaney, A. P.; Hendifar, A. E.; Pisegna, J. R.; Hecht, J. R.; Wolin, E. M.; Slavik, R.; Gupta, P.; Quon, A.; Schiepers, C.; Allen-Auerbach, M. S.; Herrmann, K. Most of the Intended Management Changes After (68)Ga-DOTATATE PET/CT Are Implemented. *J. Nucl. Med.* **2017**, *58*, 1793−1796.

(11) Zhu, W.; Cheng, Y.; Wang, X.; Yao, S.; Jia, R.; Xu, J.; Bai, C.; Zhao, H.; Huo, L. Head-to-head comparison of (68)Ga-DOTA-JR11 and (68)Ga-DOTATATE PET/CT in patients with metastatic, well-differentiated neuroendocrine tumors: a prospective study. *J. Nucl. Med.* **2019**, jnumed.119.235093.

(12) Ambrosini, V.; Nanni, C.; Fanti, S. The use of gallium-68 labeled somatostatin receptors in PET/CT imaging. *PET Clin.* **2014**, *9*, 323−9.

(13) Kulkarni, H. R.; Baum, R. P. Theranostics with Ga-68 somatostatin receptor PET/CT: monitoring response to peptide receptor radionuclide therapy. *PET Clin.* **2014**, *9*, 91−7.

(14) Taieb, D.; Garrigue, P.; Bardies, M.; Abdullah, A. E.; Pacak, K. Application and Dosimetric Requirements for Gallium-68-labeled Somatostatin Analogues in Targeted Radionuclide Therapy for Gastroenteropancreatic Neuroendocrine Tumors. *PET Clin.* **2015**, *10*, 477−86.

(15) Kanthan, G. L.; Hsiao, E.; Kneebone, A.; Eade, T.; Schembri, G. P. Desmoid Tumor Showing Intense Uptake on 68Ga PSMA-HBED-CC PET/CT. *Clin. Nucl. Med.* **2016**, *41*, 508−9.

(16) Noto, B.; Vrachimis, A.; Schafers, M.; Stegger, L.; Rahbar, K. Subacute Stroke Mimicking Cerebral Metastasis in 68Ga-PSMA-HBED-CC PET/CT. *Clin. Nucl. Med.* **2016**, *41*, No. e449.

(17) Parihar, A. S.; Sood, A.; Mittal, B. R.; Kumar, R.; Singh, H.; Dhatt, S. S. 68Ga-PSMA-HBED-CC PET/CT and 18F-FDG PET/CT in Ewing Sarcoma. *Clin. Nucl. Med.* **2020**, *45*, No. e57-e58.

(18) Verma, P.; Malhotra, G.; Goel, A.; Rakshit, S.; Chandak, A.; Chedda, R.; Banerjee, S.; Asopa, R. V. Differential Uptake of 68Ga-PSMA-HBED-CC (PSMA-11) in Low-Grade Versus High-Grade Gliomas in Treatment-Naive Patients. *Clin. Nucl. Med.* **2019**, *44*, No. e318.

(19) Pyka, T.; Weirich, G.; Einspieler, I.; Maurer, T.; Theisen, J.; Hatzichristodoulou, G.; Schwamborn, K.; Schwaiger, M.; Eiber, M. 68Ga-PSMA-HBED-CC PET for Differential Diagnosis of Suggestive Lung Lesions in Patients with Prostate Cancer. *J. Nucl. Med.* **2016**, *57*, 367−71.

(20) Damle, N. A.; Tripathi, M.; Chakraborty, P. S.; Sahoo, M. K.; Bal, C.; Aggarwal, S.; Arora, G.; Kumar, P.; Kumar, R.; Gupta, R.

Unusual Uptake of Prostate Specific Tracer (68)Ga-PSMA-HBED-CC in a Benign Thyroid Nodule. *Nucl. Med. Mol. Imaging* **2016**, *50*, 344−347.
(21) Akdemir, E. N.; Tuncel, M.; Akyol, F.; Bilen, C. Y.; Baydar, D. E.; Karabulut, E.; Ozen, H.; Caglar, M. (68)Ga-labelled PSMA ligand HBED-CC PET/CT imaging in patients with recurrent prostate cancer. *World J. Urol.* **2019**, *37*, 813−821.
(22) Schmidt, A.; Wirtz, M.; Farber, S. F.; Osl, T.; Beck, R.; Schottelius, M.; Schwaiger, M.; Wester, H. J. Effect of Carbohydration on the Theranostic Tracer PSMA I&T. *ACS Omega* **2018**, *3*, 8278−8287.
(23) Cytawa, W.; Seitz, A. K.; Kircher, S.; Fukushima, K.; Tran-Gia, J.; Schirbel, A.; Bandurski, T.; Lass, P.; Krebs, M.; Polom, W.; Matuszewski, M.; Wester, H. J.; Buck, A. K.; Kubler, H.; Lapa, C. (68)Ga-PSMA I&T PET/CT for primary staging of prostate cancer. *Eur. J. Nucl. Med. Mol. Imaging* **2020**, *47*, 168−177.
(24) Herrmann, K.; Bluemel, C.; Weineisen, M.; Schottelius, M.; Wester, H. J.; Czernin, J.; Eberlein, U.; Beykan, S.; Lapa, C.; Riedmiller, H.; Krebs, M.; Kropf, S.; Schirbel, A.; Buck, A. K.; Lassmann, M. Biodistribution and radiation dosimetry for a probe targeting prostate-specific membrane antigen for imaging and therapy. *J. Nucl. Med.* **2015**, *56*, 855−61.
(25) Meyrick, D. P.; Asokendaran, M.; Skelly, L. A.; Lenzo, N. P.; Henderson, A. The role of 68Ga-PSMA-I&T PET/CT in the pretreatment staging of primary prostate cancer. *Nucl. Med. Commun.* **2017**, *38*, 956−963.
(26) Imberti, C.; Chen, Y. L.; Foley, C. A.; Ma, M. T.; Paterson, B. M.; Wang, Y.; Young, J. D.; Hider, R. C.; Blower, P. J. Tuning the properties of tris(hydroxypyridinone) ligands: efficient (68)Ga chelators for PET imaging. *Dalton Trans.* **2019**, *48*, 4299−4313.
(27) Notni, J.; Hermann, P.; Havlickova, J.; Kotek, J.; Kubicek, V.; Plutnar, J.; Loktionova, N.; Riss, P. J.; Rosch, F.; Lukes, I. A triazacyclononane-based bifunctional phosphinate ligand for the preparation of multimeric 68Ga tracers for positron emission tomography. *Chem. - Eur. J.* **2010**, *16*, 7174−85.
(28) Waldron, B. P.; Parker, D.; Burchardt, C.; Yufit, D. S.; Zimny, M.; Roesch, F. Structure and stability of hexadentate complexes of ligands based on AAZTA for efficient PET labelling with gallium-68. *Chem. Commun.* **2013**, *49*, 579−81.
(29) Vágner, A.; D'Alessandria, C.; Gambino, G.; Schwaiger, M.; Aime, S.; Maiocchi, A.; Tóth, I.; Baranyai, Z.; Tei, L. A rigidified AAZTA-like ligand as efficient chelator for68Ga radiopharmaceuticals. *ChemistrySelect* **2016**, *1*, 163−171.
(30) Anderson, C. J.; Welch, M. J. Radiometal-labeled agents (non-technetium) for diagnostic imaging. *Chem. Rev.* **1999**, *99*, 2219−34.
(31) Poty, S.; Desogere, P.; Simecek, J.; Bernhard, C.; Goncalves, V.; Goze, C.; Boschetti, F.; Notni, J.; Wester, H. J.; Denat, F. MA-NOTMP: A Triazacyclononane Trimethylphosphinate Based Bifunctional Chelator for Gallium Radiolabelling of Biomolecules. *ChemMedChem* **2015**, *10*, 1475−9.
(32) Bollinger, J. E.; Mague, J. T.; O'Connor, C. J.; Banks, W. A.; Roundhill, D. M. Lipophilic Hexadentate Gallium, Indium and Iron Complexes of New Phenolate-Derivatized Cyclohexanetriamines as Potential in-Vivo Metal-Transfer Reagents. *J. Chem. Soc., Dalton Trans.* **1995**, 1677−1688.
(33) Derlin, T.; Schmuck, S.; Juhl, C.; Teichert, S.; Zorgiebel, J.; Wester, H. J.; Schneefeld, S. M.; Walte, A. C. A.; Thackeray, J. T.; Ross, T. L.; Bengel, F. M. Imaging Characteristics and First Experience of [(68)Ga]THP-PSMA, a Novel Probe for Rapid Kit-Based Ga-68 Labeling and PET Imaging: Comparative Analysis with [(68)Ga]PSMA I&T. *Mol. Imaging. Biol.* **2018**, *20*, 650−658.
(34) de Sa, A.; Matias, A. A.; Prata, M. I.; Geraldes, C. F.; Ferreira, P. M.; Andre, J. P. Gallium labeled NOTA-based conjugates for peptide receptor-mediated medical imaging. *Bioorg. Med. Chem. Lett.* **2010**, *20*, 7345−8.
(35) Schmidtke, A.; Lappchen, T.; Weinmann, C.; Bier-Schorr, L.; Keller, M.; Kiefer, Y.; Holland, J. P.; Bartholoma, M. D. Gallium Complexation, Stability, and Bioconjugation of 1,4,7-Triazacyclononane Derived Chelators with Azaheterocyclic Arms. *Inorg. Chem.* **2017**, *56*, 9097−9110.
(36) Baranyai, Z.; Uggeri, F.; Maiocchi, A.; Giovenzana, G. B.; Cavallotti, C.; Takacs, A.; Toth, I.; Banyai, I.; Benyei, A.; Brucher, E.; Aime, S. Equilibrium, Kinetic and Structural Studies of AAZTA Complexes with Ga3+, In3+ and Cu2+. *Eur. J. Inorg. Chem.* **2013**, *2013*, 147−162.
(37) Farkas, E.; Nagel, J.; Waldron, B. P.; Parker, D.; Toth, I.; Brucher, E.; Rosch, F.; Baranyai, Z. Equilibrium, Kinetic and Structural Properties of Gallium(III) and Some Divalent Metal Complexes Formed with the New DATA(m) and DATA(5m) Ligands. *Chem. - Eur. J.* **2017**, *23*, 10358−10371.
(38) Boros, E.; Ferreira, C. L.; Cawthray, J. F.; Price, E. W.; Patrick, B. O.; Wester, D. W.; Adam, M. J.; Orvig, C. Acyclic Chelate with Ideal Properties for Ga-68 PET Imaging Agent Elaboration. *J. Am. Chem. Soc.* **2010**, *132*, 15726−15733.
(39) Eder, M.; Schafer, M.; Bauder-Wust, U.; Hull, W. E.; Wangler, C.; Mier, W.; Haberkorn, U.; Eisenhut, M. 68Ga-complex lipophilicity and the targeting property of a urea-based PSMA inhibitor for PET imaging. *Bioconjugate Chem.* **2012**, *23*, 688−97.
(40) Andre, J. P.; Maecke, H. R.; Andre, J. P.; Zehnder, M.; Macko, L.; Akyel, K. G. 1,4,7-triazacyclononane-1-succinic acid-4,7-diacetic acid (NODASA): A new bifunctional chelator for radio gallium-labelling of biomolecules. *Chem. Commun.* **1998**, 1301−1302.
(41) Wang, X.; Jaraquemada-Peláez, M. d. G.; Cao, Y.; Pan, J.; Lin, K.-S.; Patrick, B. O.; Orvig, C. H_2hox: Dual-Channel Oxine-Derived Acyclic Chelating Ligand for (68)Ga Radiopharmaceuticals. *Inorg. Chem.* **2019**, *58*, 2275−2285.
(42) Forster, G. J.; Engelbach, M. J.; Brockmann, J. J.; Reber, H. J.; Buchholz, H. G.; Macke, H. R.; Rosch, F. R.; Herzog, H. R.; Bartenstein, P. R. Preliminary data on biodistribution and dosimetry for therapy planning of somatostatin receptor positive tumours: comparison of (86)Y-DOTATOC and (111)In-DTPA-octreotide. *Eur. J. Nucl. Med. Mol. Imaging* **2001**, *28*, 1743−50.
(43) Camera, L.; Kinuya, S.; Garmestani, K.; Brechbiel, M. W.; Wu, C.; Pai, L. H.; McMurry, T. J.; Gansow, O. A.; Pastan, I.; Paik, C. H.; Carrasquillo, J. A. Evaluation of the serum stability and in vivo biodistribution of CHX-DTPA and other ligands for yttrium labeling of monoclonal antibodies. *J. Nucl. Med.* **1994**, *35*, 882−889.
(44) Price, E. W.; Orvig, C. Matching chelators to radiometals for radiopharmaceuticals. *Chem. Soc. Rev.* **2014**, *43*, 260−90.
(45) Kostelnik, T. I.; Orvig, C. Radioactive Main Group and Rare Earth Metals for Imaging and Therapy. *Chem. Rev.* **2019**, *119*, 902−956.
(46) Chong, H. S.; Garmestani, K.; Ma, D.; Milenic, D. E.; Overstreet, T.; Brechbiel, M. W. Synthesis and biological evaluation of novel macrocyclic ligands with pendent donor groups as potential yttrium chelators for radioimmunotherapy with improved complex formation kinetics. *J. Med. Chem.* **2002**, *45*, 3458−64.
(47) Brechbiel, M. W.; Gansow, O. A.; Pippin, C. G.; Rogers, R. D.; Planalp, R. P. Preparation of the Novel Chelating AgentN-(2-Aminoethyl)-trans-1,2-diaminocyclohexane-N,N′,N″-pentaacetic Acid (H5CyDTPA), a Preorganized Analogue of Diethylenetriaminepenta-acetic Acid (H5DTPA), and the Structures of BiIII(CyDTPA)2-and BiIII(H2DTPA) Complexes. *Inorg. Chem.* **1996**, *35*, 6343−6348.
(48) Stimmel, J. B.; Stockstill, M. E.; Kull, F. C. Yttrium-90 Chelation Properties of Tetraazatetraacetic Acid Macrocycles, Diethylenetriaminepentaacetic Acid Analogs, and a Novel Terpyridine Acyclic Chelator. *Bioconjugate Chem.* **1995**, *6*, 219−225.
(49) Mouralian, C.; Buss, J. L.; Stranix, B.; Chin, J.; Ponka, P. Mobilization of iron from cells by hydroxyquinoline-based chelators. *Biochem. Pharmacol.* **2005**, *71*, 214−222.
(50) Wang, X.; Jaraquemada-Pelaez, M. d. G.; Rodriguez-Rodriguez, C.; Cao, Y.; Buchwalder, C.; Choudhary, N.; Jermilova, U.; Ramogida, C. F.; Saatchi, K.; Häfeli, U. O.; Patrick, B. O.; Orvig, C. H4octox: Versatile Bimodal Octadentate Acyclic Chelating Ligand for Medicinal Inorganic Chemistry. *J. Am. Chem. Soc.* **2018**, *140*, 15487−15500.

https://dx.doi.org/10.1021/acs.inorgchem.0c00168
Inorg. Chem. 2020, 59, 4895−4908

(51) Ramogida, C. F.; Cawthray, J. F.; Boros, E.; Ferreira, C. L.; Patrick, B. O.; Adam, M. J.; Orvig, C. H2CHXdedpa and H4CHXoctapa - chiral acyclic chelating ligands for 67/68Ga and 111In radiopharmaceuticals. *Inorg. Chem.* **2015**, *54*, 2017−2031.
(52) Gans, P.; Sabatini, A.; Vacca, A. Determination of equilibrium constants from spectrophotometric data obtained from solutions of known pH: The program pHab. *Ann. Chim.* **1999**, *89*, 45−49.
(53) Kubicek, V.; Havlickova, J.; Kotek, J.; Tircso, G.; Hermann, P.; Toth, E.; Lukes, I. Gallium(III) complexes of DOTA and DOTA-monoamide: kinetic and thermodynamic studies. *Inorg. Chem.* **2010**, *49*, 10960−9.
(54) Ramogida, C. F.; Boros, E.; Patrick, B. O.; Zeisler, S. K.; Kumlin, J.; Adam, M. J.; Schaffer, P.; Orvig, C. Evaluation of H2CHXdedpa, H2dedpa- and H2CHXdedpa-N,N'-propyl-2-NI ligands for (64)Cu(II) radiopharmaceuticals. *Dalton Trans.* **2016**, *45*, 13082−90.
(55) Sephton, R. G.; Hodgson, G. S.; De Abrew, S.; Harris, A. W. Ga-67 and Fe-59 distributions in mice. *J. Nucl. Med.* **1978**, *19*, 930−935.
(56) Autio, A.; Virtanen, H.; Tolvanen, T.; Liljenback, H.; Oikonen, V.; Saanijoki, T.; Siitonen, R.; Kakela, M.; Schussele, A.; Teras, M.; Roivainen, A. Absorption, distribution and excretion of intravenously injected (68)Ge/ (68)Ga generator eluate in healthy rats, and estimation of human radiation dosimetry. *EJNMMI Res.* **2015**, *5*, 117.
(57) Thews, O.; Zimny, M.; Eppard, E.; Piel, M.; Bausbacher, N.; Nagel, V.; Rosch, F. In vitro and in vivo structure-property relationship of (68)Ga-labeled Schiff base derivatives for functional myocardial pet imaging. *Mol. Imaging. Biol.* **2014**, *16*, 802−12.
(58) Boros, E.; Ferreira, C. L.; Patrick, B. O.; Adam, M. J.; Orvig, C. New Ga derivatives of the H_2dedpa scaffold with improved clearance and persistent heart uptake. *Nucl. Med. Biol.* **2011**, *38*, 1165−74.
(59) Hsiao, Y. M.; Mathias, C. J.; Wey, S. P.; Fanwick, P. E.; Green, M. A. Synthesis and biodistribution of lipophilic and monocationic gallium radiopharmaceuticals derived from N,N'-bis(3-aminopropyl)-N,N'-dimethylethylenediamine: potential agents for PET myocardial imaging with 68Ga. *Nucl. Med. Biol.* **2009**, *36*, 39−45.
(60) Plossl, K.; Chandra, R.; Qu, W.; Lieberman, B. P.; Kung, M. P.; Zhou, R.; Huang, B.; Kung, H. F. A novel gallium bisaminothiolate complex as a myocardial perfusion imaging agent. *Nucl. Med. Biol.* **2008**, *35*, 83−90.
(61) Kim, Y. S.; Wang, F.; Liu, S. Minimizing liver uptake of cationic Tc radiotracers with ether and crown ether functional groups. *World J. Hepatol.* **2010**, *2*, 21−31.
(62) Ramogida, C. F.; Schindler, D.; Schneider, C.; Tan, Y. L. K.; Huh, S.; Ferreira, C. L.; Adam, M. J.; Orvig, C. Synthesis and characterization of lipophilic cationic Ga(III) complexes based on the H(2)CHXdedpa and H(2)dedpa ligands and their Ga-67/68 radiolabeling studies. *RSC Adv.* **2016**, *6*, 103763−103773.
(63) Eder, M.; Neels, O.; Muller, M.; Bauder-Wust, U.; Remde, Y.; Schafer, M.; Hennrich, U.; Eisenhut, M.; Afshar-Oromieh, A.; Haberkorn, U.; Kopka, K. Novel Preclinical and Radiopharmaceutical Aspects of [68Ga]Ga-PSMA-HBED-CC: A New PET Tracer for Imaging of Prostate Cancer. *Pharmaceuticals* **2014**, *7*, 779−96.
(64) Wirtz, M.; Schmidt, A.; Schottelius, M.; Robu, S.; Gunther, T.; Schwaiger, M.; Wester, H. J. Synthesis and in vitro and in vivo evaluation of urea-based PSMA inhibitors with increased lipophilicity. *EJNMMI Res.* **2018**, *8*, 84.
(65) Lin, K.-S.; Pan, J.; Amouroux, G.; Turashvili, G.; Mesak, F.; Hundal-Jabal, N.; Pourghiasian, M.; Lau, J.; Jenni, S.; Aparicio, S.; Bénard, F. In Vivo Radioimaging of Bradykinin Receptor B1, a Widely Overexpressed Molecule in Human Cancer. *Cancer Res.* **2015**, *75*, 387−393.
(66) Yanai, T.; Tew, D. P.; Handy, N. C. A new hybrid exchange−correlation functional using the Coulomb-attenuating method (CAM-B3LYP). *Chem. Phys. Lett.* **2004**, *393*, 51−57.
(67) Scalmani, G.; Frisch, M. J. Continuous surface charge polarizable continuum models of solvation. I. General formalism. *J. Chem. Phys.* **2010**, *132*, 114110.
(68) Wadt, W. R.; Hay, P. J. Ab initio effective core potentials for molecular calculations. Potentials for main group elements Na to Bi. *J. Chem. Phys.* **1985**, *82*, 284−298.
(69) Paul, M. A.; Long, F. A. H^0 and related indicator acidity function. *Chem. Rev.* **1957**, *57*, 1−45.
(70) Weekes, D. M.; Ramogida, C. F.; Jaraquemada-Pelaez, M. d. G.; Patrick, B. O.; Apte, C.; Kostelnik, T. I.; Cawthray, J. F.; Murphy, L.; Orvig, C. Dipicolinate Complexes of Gallium(III) and Lanthanum-(III). *Inorg. Chem.* **2016**, *55*, 12544−12558.
(71) Gran, G. Determination of the equivalence point in potentiometric titrations. Part II. *Analyst* **1952**, *77*, 661−671.
(72) Baes, C. F., Jr.; Mesmer, R. E. *The Hydrolysis of Cations*; John Wiley & Sons: New York, 1976.
(73) Harris, W. R.; Carrano, C. J.; Raymond, K. N. Spectrophotometric Determination of the Proton-Dependent Stability Constant of Ferric Enterobactin. *J. Am. Chem. Soc.* **1979**, *101*, 2213−2214.
(74) Freshney, R. I.; Capes-Davis, A.; Gregory, C.; Przyborski, S. *Culture of Animal Cells: A Manual of Basic Technique and Specialized Applications*,seventh ed.;Wiley Blackwell: Hoboken, NJ, 2016.
(75) Langdon, S. P. *Cancer Cell Culture: Methods and Protocols*; Humana Press: Totowa, NJ, 2004.

https://dx.doi.org/10.1021/acs.inorgchem.0c00168
Inorg. Chem. 2020, 59, 4895−4908